

1                   **Analyzing ozone variations and uncertainties at high latitudes during Sudden**  
2                   **Stratospheric Warming events using MERRA-2**

3                   **Shima Bahramvash Shams**<sup>1,2</sup>, Von P. Walden<sup>1</sup>, James W Hannigan<sup>2</sup>, William J. Randel<sup>2</sup>, Irina  
4 V. Petropavlovskikh<sup>3,4</sup>, Amy H. Butler<sup>5</sup>, Alvaro de la Cámara<sup>6</sup>

5  
6                   <sup>1</sup> Washington State University, Pullman, WA, United States,

7                   <sup>2</sup> NCAR, National Center for Atmospheric Research, Boulder, CO, United States,

8                   <sup>3</sup> Cooperative Institute for Research in Environmental Sciences, University of Colorado, Boulder, CO, USA

9                   <sup>4</sup> National Oceanic and Atmospheric Administration, Global Monitoring Division, Boulder, CO, USA

0                   <sup>5</sup> National Oceanic and Atmospheric Administration, Chemical Sciences Laboratory, Boulder, CO, USA

1                   <sup>6</sup> Dept. Física de la Tierra y Astrofísica, Universidad Complutense de Madrid, Madrid, Spain  
2

3                   **Abstract:**

4                   Stratospheric circulation is a critical part of the Arctic ozone cycle. Sudden stratospheric warming  
5 events (SSWs) manifest the strongest alteration of stratospheric dynamics. During SSWs, changes in  
6 planetary wave propagation vigorously influence zonal mean zonal wind, temperature, and tracer  
7 concentrations in the stratosphere over the high latitudes. In this study, we examine six persistent major  
8 SSWs from 2004 to 2020 using the Modern-Era Retrospective analysis for Research and Applications,  
9 Version 2 (MERRA-2). Using the unique density of observations around the Greenland sector at high  
10 latitudes, we perform comprehensive comparisons of high latitude observations with the MERRA-2  
11 ozone dataset during the six major SSWs. Our results show that MERRA-2 captures the high variability  
12 of mid stratospheric ozone fluctuations during SSWs over high latitudes. However, larger uncertainties  
13 are observed in the lower stratosphere and troposphere. The zonally averaged stratospheric ozone shows  
14 a dramatic increase of 9-29% in total column ozone (TCO) near the time of each SSW, which lasts up to  
15 two months. This study shows that the average shape of the Arctic polar vortex before SSWs influences  
16 the geographical extent, timing, and magnitude of ozone changes. The SSWs exhibit a more significant

1 impact on ozone over high northern latitudes when the average polar vortex is mostly elongated as seen  
2 in 2009 and 2018 compared to the events in which the polar vortex is displaced towards Europe. Strong  
3 correlation ( $R^2=90\%$ ) is observed between the magnitude of change in average equivalent potential  
4 vorticity before and after SSWs and the associated averaged total column ozone changes over high  
5 latitudes. This paper investigates the different terms of the ozone continuity equation using MERRA-2  
6 circulation, which emphasizes the key role of vertical advection on mid-stratospheric ozone during the  
7 SSWs and the magnified vertical advection in elongated vortex shape as seen in 2009 and 2018.

## 8 1. Introduction

9 Stratospheric ozone can modulate the radiative forcing of climate and Earth's surface temperature  
0 (Haigh, 1994; Ramaswamy et al., 1996; Smith and Polvani, 2014; Calvo et al., 2015; Kidston et al., 2015;  
1 Nowack et al., 2015; Romanowsky et al., 2019). High latitude stratospheric ozone influences tropospheric  
2 climate, surface temperature of lower latitudes, El Niño-Southern Oscillation (ENSO) events, and the  
3 North Pacific Oscillation (NPO) (Baldwin and Dunkerton, 2001; Ineson and Scaife, 2008; Cagnazzo and  
4 Manzini, 2009; Karpechko et al., 2014; Xie et al., 2016). Thus, it is important to have a thorough  
5 understanding of high latitude ozone variations.

6 Dynamical variability plays a critical role in fluctuations of stratospheric ozone (Holton et al.,  
7 1995; Fusco and Salby, 1999; Rao et al., 2004; Bahramvash-Shams et al., 2019). Planetary waves  
8 modulate poleward ozone transport through the Brewer-Dobson circulation (BDC) (Lindzen and Holton,  
9 1968; Holton and Lindzen, 1972; Wallace, 1973; Holton et al., 1995). High latitude ozone accumulation  
10 during winter and peak values in the spring are largely controlled by BDC transport of ozone-rich, tropical  
11 stratospheric air (Rao, 2003; Rao et al., 2004). Sudden stratospheric warming events (SSWs) are the  
12 largest alterations of stratospheric circulation during wintertime and significantly influence the  
13 interannual variability of stratospheric transport (Schoeberl, 1978; Butler et al., 2015; de la Cámara et al.,  
14 2018a; Baldwin et al., 2021).

15 SSWs are defined by a reversal of the climatological westerly wind circulation, which typically  
16 coincides with an abrupt and intense stratospheric temperature increase (Scherhag, 1952, Baldwin et al.  
17 2021). Although the current understanding of the mechanisms that induce SSWs is still uncertain (de la

1 Cámara et al., 2019; Lawrence and Manney, 2020), increased vertical propagation of planetary-scale  
2 waves from the extratropical troposphere into the stratosphere over high latitudes is closely related to  
3 these abrupt events (Matsuno, 1971; Schoeberl, 1978; Scott and Polvani, 2004). However, the occurrence  
4 of SSWs is shown to be sensitive to many other factors such as lower stratosphere conditions, the  
5 geometry of the polar vortex, the gradient of potential vorticity (PV) at the edge of the polar vortex, and  
6 synoptic systems at lower altitudes (Tripathi et al. 2015, de la Cámara et al., 2019; Lawrence and Manney,  
7 2020). Changes in momentum deposition associated with these dynamical states lead to the rapid  
8 deceleration and disruption of the stratospheric polar vortex, typically by either splitting the vortex into  
9 two smaller lobes or displacing the vortex off the pole (Matsuno, 1971; Polvani and Waugh, 2004;  
0 Charlton and Polvani, 2007). The altered circulation during SSWs impacts the transport of trace gases  
1 (Randel 1993, de la Cámara et al., 2018b), tropospheric weather and climate (Baldwin and Dunkerton,  
2 2001; Butler et al., 2017; Charlton-Perez et al., 2018, Butler and Domeisen 2021), and gravity waves  
3 over the Arctic (Thurairajah et al., 2010) and consequently the pole-to-pole circulation (Houghton, 1978;  
4 Fritts and Alexander, 2003). SSWs are some of the strongest manifestations of atmospheric coupling.  
5 These large-scale altered circulations perturb the mesosphere by cooling it and consequently lowering  
6 the stratopause by up to 30 km (Manney et al., 2008b). Dynamical coupling between the stratosphere and  
7 troposphere is another important consequence of SSWs with implications for surface climate  
8 predictability on subseasonal timescales (Baldwin and Dunkerton 2001, Butler et al. 2019).

9 From 2004 to 2020, six major SSWs persisted (persistent easterly winds at 60°N 10hPa) for more  
10 than two weeks with each of these events having significant impacts on Arctic ozone. Since 2004, the  
11 number of stratospheric observations has increased, and various studies have focused on individual  
12 SSWs, their evolution, and their impact on trace gases. For example, Siskind et al. 2007 investigated trace  
13 gas (CO) descent from mesosphere to the upper stratospheric layers during the SSW event in 2006, using  
14 the Navy Operational Global Atmospheric Prediction System–Advanced Level Physics, High Altitude  
15 (NOGAPS-ALPHA) model, along with observations from the Sounding of the Atmosphere with  
16 Broadband Emission Radiometry (SABER). Manney et al. (2008a) investigated the evolution of the  
17 SSWs in 2004 (minor) and 2006 by focusing on the transport of traces gases, including CO, H<sub>2</sub>O, and  
18 N<sub>2</sub>O using Microwave Limb Sounder (MLS), SABER, and ACE-Fourier Transform Spectrometer (ACE-  
19 FTS) at Eureka Canada. The evolution of the 2008 SSW and its associated changes in ozone and water

1 vapor over northern Europe and, specifically, Bern, Switzerland was studied using the ground-based  
2 microwave radiometer and ozone spectrometer measurements, as well as MLS and Cloud-Aerosol Lidar  
3 and Infrared Pathfinder Satellite Observations (CALIPSO) measurements and meteorological data from  
4 reanalysis systems (Flury et al. 2009).

5 Manney et al. (2009b) used MLS and GEOS-5 data to discuss the dynamics and evolution of trace  
6 gas transport ( $\text{CO}$ ,  $\text{N}_2\text{O}$ ,  $\text{H}_2\text{O}$ ) during the 2009 SSW event with a split polar vortex and compared it to  
7 the 2006 SSW with a displaced vortex. They confirmed a more rapid changes in trace gases during the  
8 split vortex event compared to displaced vortex, similar to a previous study by Charlton and Polvani  
9 (2007). Tao et al, (2015) showed the significant impact of dynamical forcing in variability of  $\text{N}_2\text{O}$  and  
0  $\text{O}_3$  during the SSW in 2009, using chemical Lagrangian Model of the Stratosphere (CLaMS) simulations  
1 and tracer-tracer correlation.

2 Using CALIPSO and trace gas data ( $\text{N}_2\text{O}$ ,  $\text{HCL}$ ,  $\text{HNO}_3$ ,  $\text{CLO}$ , and  $\text{O}_3$ ) from MLS, and MERRA  
3 meteorological fields, Manney et al. (2015) showed that during the 2013 SSW, the persistent spring  
4 vortex, after it split in the lower latitudes and was exposed to sunlight, caused record ozone depletion in  
5 the Northern Hemisphere. Schranz et al. (2020) investigate the impact of the SSW in 2019 on ozone and  
6  $\text{H}_2\text{O}$  over Ny-Ålesund, Norway, in particular, and the northern hemisphere, in general, by analyzing the  
7 ground-based microwave radiometers, MLS measurements, MERRA-2 and climate simulations.

8 de la Cámara et al. (2018) analyzed the climatological impact of SSWs and their associated  
9 changes in stratospheric transport using ERAI reanalysis and WACCM simulations. They showed the  
10 associated changes in residual circulation and isentropic mixing and emphasized the impact of mixing on  
11 atmospheric composition in the lower stratosphere. The composite mean ozone changes during SSWs  
12 and associated chemical and dynamical conditions is also discussed by de la Cámara et al. (2018b).

13 While the above summarizes the studies that have looked at individual or composite SSW events  
14 the relative magnitude and extent of these events and their specific impact on ozone have not been  
15 compared to each other. How do the observed changes in Arctic ozone during each of the SSWs compare  
16 with the simulated climatology? If there are major differences associated with these events, do they fit  
17 into certain categories? What physical parameters modulate the different impacts of SSWs on Arctic

1 ozone?

2 To our knowledge, no previous study has investigated these questions. Therefore, this study  
3 investigates the dynamical variability and ozone variations at northern high latitudes (between 60°N and  
4 80°N) using the MERRA-2 dataset, both in the zonal average and within a specific geographical region  
5 during six persistent, major SSWs. We show that the magnitude, geographical extent, and timing of ozone  
6 changes are connected more closely to the averaged polar vortex shape before the SSW event rather than  
7 the final form of the vortex after breakdown (split vs displacement). We also show there is strong  
8 correlation between changes in average equivalent potential vorticity (EPV) and ozone column changes  
9 during these SSWs at high northern latitudes.

0 The Modern Era Retrospective Analysis for Research and Application, version 2 (MERRA-2) is  
1 used to investigate ozone fluctuations during SSWs. Previous validation of MERRA-2 ozone data with  
2 ozonesondes and satellite data over the South Pole and midlatitudes has shown good correlation (Gelaro  
3 et al., 2017; Wargan et al., 2017). However, MERRA-2 ozone data are expected to have higher  
4 uncertainties over the northern high latitudes because of higher dynamic variability in this region (Wargan  
5 et al., 2017). During SSWs, the alteration of dynamical processes causes dramatic variability in trace gas  
6 concentrations in the middle atmosphere. The complexity of altered dynamics of SSWs might introduce  
7 extra uncertainties into numerical models and data assimilation systems. The performance of MERRA-2  
8 ozone products during SSWs has not been investigated in previous studies. It is essential to understand  
9 the performance of MERRA-2 ozone during these anomalous events before using them for further  
:0 analysis of ozone variations

:1 This study focuses on using observations and assimilation data to analyze and compare the impact  
:2 of persistent major SSWs on ozone from 2004 to 2020. During SSWs, MERRA-2 ozone data are  
:3 compared with in situ and ground-based remote sensing observations from high northern latitudes. The  
:4 advantage of an existing dense network of observations around the Greenland sector at high latitudes  
:5 (Figure 1) provides an opportunity to explore the uncertainties of MERRA-2 ozone profiles over high  
:6 latitudes during SSWs. These comparisons provide a thorough understanding of the uncertainties in the  
:7 MERRA-2 dataset in this region and, in particular, during extreme dynamic events.

1 In section 2, MERRA-2 and other independent observations are described. The methodology of  
2 comparisons and dynamical analysis are presented in section 3. The results of the comparison between  
3 MERRA-2 and independent observation are discussed in section 4. The evolution of each SSW and its  
4 impact on ozone are discussed in section 5. Discussion of transport mechanisms of ozone is provided in  
5 section 6. Section 7 presents the conclusions of this research study.

## 6 **2. Data**

7 The Modern-Era Retrospective Analysis for Research and Application, version 2 (MERRA-2)  
8 from NASA's Global Monitoring and Assimilation Office (GMAO) uses the GEOS-5 atmospheric data  
9 assimilation system (Molod et al., 2015; Gelaro et al., 2017). A variety of data sets are incorporated into  
0 a general circulation model to create 3-dimensional MERRA-2 ozone datasets with a time-frequency of  
1 3 hours (Wargan et al., 2017; Gelaro et al., 2017). Total column ozone from the Solar Backscatter  
2 Ultraviolet Radiometer (SBUV) (1980 to 2004) and the Ozone Monitoring Instrument (OMI) (since  
3 2004) and retrieved ozone profiles from SBUV (1980 to 2004) and the MLS (since August 2004, down  
4 to 177 hPa to 2015, down to 215 hPa after 2015) are used to estimate ozone in MERRA-2 (Gelaro et al.,  
5 2017).

6 MERRA-2 data are available online through the NASA Goddard Earth Sciences Data Information  
7 Services Center (GES DISC; <http://disc.sci.gsfc.nasa.gov/daac-bin/DataHoldings.pl>). MERRA-2 has  
8 been used to study ozone trends and processes (Coy et al., 2016; Knowland et al., 2017; Wargan et al.,  
9 2018; Albers et al., 2018; Shangguan et al., 2019). In this study, the ozone dataset from the MERRA-2  
10 reanalyses at a spatial resolution of  $0.5^\circ \times 0.625^\circ$  will be used. To have the finest possible vertical  
11 resolution for the comparisons with observations, MERRA-2 ozone at the model levels is used (GMAO,  
12 2015a). Other dynamical variables such as temperature, and the northward and vertical wind velocities  
13 ( $v$ ,  $\omega$ ), are extracted from the pressure-level MERRA-2 dataset (GMAO, 2015b), which facilitates the  
14 calculation of variables such as potential vorticity (PV) and potential temperature ( $\theta$ ).

15 In reanalysis products such as MERRA-2, methods of analysis, model uncertainties, and  
16 observations cause uncertainties in the products (Rienecker et al. 2011). MERRA-2 is shown to have the  
17 best agreement with stratospheric ozone observations compared to other reanalysis data (Davis et al,

1 2017). Previously MERRA-2 ozone data was validated using ozonesondes and satellite data from 2005  
2 to 2012 (Gelaro et al., 2017; Wargan et al., 2017). MERRA-2 agreement with independent observations  
3 has been improved since 2005 by assimilating OMI and MLS. Comparison with independent satellite  
4 observations show an average standard deviation of the differences of 5% and 11% in the upper and lower  
5 stratosphere, respectively (Wargan et al., 2017). The average standard deviation of 20% has been reported  
6 for the comparison between MERRA-2 lower stratospheric ozone and ozonesondes (Wargan et al., 2017).  
7 However, uncertainties are expected to be magnified at high latitudes because of higher dynamical  
8 variability (Wargan et al., 2017). Moreover, the anomalous atmospheric dynamics, displaced/split polar  
9 vortex, and hemispherically asymmetric conditions during SSWs may cause complexity and additional  
0 uncertainties in estimation of ozone flux/transport terms. Thus, it is important to investigate the quality  
1 of MERRA-2 ozone simulations during highly altered circulations such as SSWs. This study provides a  
2 comprehensive comparison using ground-based remote sensing and in situ observations to MERRA-2  
3 ozone datasets over northern high latitudes during SSWs.

4 We use a uniquely dense network of observations in the high latitudes to study a region of the  
5 Arctic that is climatologically important in terms of stratospheric circulation (Figure 1). Ozonesondes  
6 have been used to monitor ozone for decades as the most direct measurement of the vertical ozone profile  
7 (Tiao et al., 1986; Logan, 1994; Logan et al., 1999; Stolarski, 2001; Gaudel et al., 2015; Bahramvash-  
8 Shams et al., 2019). Ozonesonde profiles provide a good standard for validation because they have high  
9 accuracy, fine vertical resolution of less than 100 m, year-round launches, and low sensitivity to clouds  
0 (McDonald et al., 1999; Ancellet et al., 2016; Sterling et al., 2017).

1 In this study, ozonesonde measurements at Eureka, Ny-Ålesund, Thule, and Summit will be used  
2 to investigate the uncertainties of MERRA-2. The locations of each station and the length of the  
3 ozonesonde measurements at each site are shown in Figure 1 and Table I. Most of the ozonesonde  
4 measurements can be found at the World Ozone and Ultraviolet Radiation Data Centre (WOUDC), while  
5 ozonesonde data in the United States is obtained from NOAA's Earth System Research Laboratory  
6 including data from Summit Station, Greenland. The detailed description and uncertainty estimation of  
7 ozonesonde measurements have been discussed in previous studies (Komhyr, 1986; Johnson et al., 2002;  
8 Smit et al., 2007; Tarasick et al., 2016; Sterling et al., 2017).

1 In addition to ozonesondes, ground-based remote sensing data are also used in this paper to study  
2 the uncertainties in the MERRA-2 dataset. Retrieved ozone from ground-based Fourier transform infrared  
3 (FTIR) interferometers have been used for long term ozone analysis (Vigouroux et al., 2008; García et  
4 al., 2012; Vigouroux et al., 2015). In this study, ozone profiles retrieved from FTIR at five high-latitude  
5 sites (Eureka, Ny-Ålesund, Thule, Harestua, and Kiruna) were obtained from NDACC (Network for the  
6 Detection of Atmospheric Composition Change) and used to validate MERRA-2. The location of each  
7 site is shown in Figure 1 and Table I. These datasets are available at <http://www.ndacc.org>.

8 The NDACC FTIR instruments measure solar radiation in a wide spectral bandwidth of 600-4500  
9  $\text{cm}^{-1}$  at a high spectral resolution of  $0.0035 \text{ cm}^{-1}$ . The retrieval of ozone profiles from NDACC FTIR  
0 instruments uses the optimal estimation method (Rodgers, 2000). NDACC retrievals use the  
1 spectroscopic database from HITRAN 2008 (Rothman et al., 2009). To retrieve trace gas information  
2 from the measured spectra using optimal estimation, additional information is required to constrain the  
3 result and find the optimal answer. Meteorological parameters from the National Centers for  
4 Environmental Prediction (NCEP) and monthly trace gas profiles from the Whole Atmosphere  
5 Community Climate Model WACCM4 (Marsh et al., 2013) are used as prior conditions. More details of  
6 the NDACC ozone retrieval steps, configuration, and instrument specifications are discussed by  
7 Vigouroux et al (2008; 2015). These instruments require sunlight and clear-sky conditions, which restricts  
8 observations to the polar day at high latitudes.

9 The retrieved total ozone column and the stratospheric partial columns from FTIR are expected  
10 to have uncertainties of 2% and 6%, respectively (Vigouroux et al., 2015). This study updates the  
11 uncertainties found by previous studies by adding additional years of data and by focusing on three high  
12 latitude sites that contain both ozonesondes and FTIR measurements. The FTIR ozone retrievals showed  
13 a high correlation ( $\sim 90\%$ ) in comparison to ozonesonde profiles measured at Eureka, Ny-Ålesund, and  
14 Thule, with uncertainties shown in Table I. Overall, the uncertainties are slightly higher than the averaged  
15 uncertainties reported by Vigouroux et al (2015). This is more pronounced at Eureka due to the high solar  
16 zenith angle, and the possibility that, at times, the FTIR views a slant path through the atmosphere that  
17 extends through the edge of the polar vortex. More details on the ozone retrievals at Eureka can be found  
18 in Bognar et al (2019). As shown in Table I, the NDACC retrievals are biased high when compared to



1 the ozonesondes. Also, the bias is higher at Eureka (7%) than at either Ny-Ålesund (1%) and Thule (3%).  
2 These biases and standard deviations (shown in table I) are less than the differences between MERRA-2  
3 and the ozonesondes (20%) discussed above, indicating that the NDACC FTIR ozone retrievals can be  
4 used to increase the robustness of the uncertainty analysis of the MERRA-2 ozone dataset.

### 5 3. Methods

6 In this section, the details of the different methods used in this study are discussed, including the  
7 comparison methodology, detection of SSWs, and the derivation of dynamical parameters used to  
8 investigate ozone transport.

9 To have comparable points, NDACC and in situ site locations, shown in Figure 1 and Table I, are  
0 extracted from the nearest  $0.5^\circ \times 0.625^\circ$  grid MERRA-2 ozone dataset. The nearest instantaneous 3-hourly  
1 MERRA-2 ozone dataset is compared to the associated ozonesonde profile and the FTIR-retrieved ozone.  
2 The MERRA-2 ozone data are compared to ozonesondes at the model levels, up to the maximum  
3 measured altitude. Since the vertical resolution of the FTIR retrieval does not match to the vertical  
4 resolution of the assimilation system, a more direct comparison involves a convolution of the reanalysis  
5 profiles using the FTIR averaging kernel (Rodgers and Connor, 2003). Averaging kernels characterize  
6 the vertical resolution and sensitivity of FTIR instruments to the atmospheric ozone variability at various  
7 altitudes (Rodgers, 2000). Equation 1 shows how the averaging kernel is applied with the reanalysis data  
8 to account for the sensitivity of retrievals (Rodgers and Connor, 2003), producing a smoothed ozone  
9 profile.

$$10 \quad x_s = x_a + A (x_h - x_a) \quad (1)$$

11 where  $x_s$  is the final smoothed profile,  $x_h$  is the reanalysis estimated profile, and  $x_a$  and  $A$  are the  
12 a priori and averaging kernel of ozone mixing ratio for the retrieval respectively. The smoothing method  
13 effectively applies the sensitivity of the retrieval to the ozone mixing ratio profile from the reanalysis  
14 using the averaging kernel and the priori information to create comparable profiles. (Rodgers and Connor,  
15 2003). MERRA-2 data are interpolated to the vertical grid of the retrievals before Equation 1 is applied.

16 The high spectral resolution of the solar FTIR measurements makes it possible to retrieve partial  
9

1 ozone columns in addition to the total column ozone. Based on the mean average kernels at all 5 stations,  
 2 four partial column ozone (PCO) are determined in this study over the following altitude regions: ground-  
 3 8 km, 8-15 km, 15-22 km, 22-34 km. The PCO amounts are also used to analyze uncertainties in the  
 4 MERRA-2 ozone dataset. The comparison results are discussed in section 4.

5 There are a variety of definitions for detecting major SSWs (Charlton & Polvani, 2007; Butler et  
 6 al., 2015; Palmeiro et al. 2015). This study uses wintertime reversals of the daily-mean, zonal-mean zonal  
 7 winds at 60N and 10 hPa from the MERRA-2 dataset (Butler et al., 2017). The dates of major SSWs  
 8 since August 2004 (MLS data incorporation into MERRA-2) are calculated using MERRA-2 data  
 9 following the method described by Charlton & Polvani (2007). This paper focuses on six persistent mid-  
 0 winter (December-February) major warmings in this period that exhibited persistent easterly zonal mean  
 1 zonal winds with a duration of at least 16 days (Table II). Table II includes the duration, magnitude of  
 2 the easterly zonal wind, and the duration of polar vortex recovery for each SSW; all information is derived  
 3 from MERRA-2 data. It should be noted that the duration of the easterly wind shown in Table II is not  
 4 necessarily consecutive. Two major SSWs during the 2004-2020 time period are not included in the main  
 5 results of our study because they did not meet the persistence criteria. The major SSW in 2007 exhibits  
 6 only 4 days of easterly zonal mean zonal winds, while the major SSW in Feb 2010 exhibits only 9 days.  
 7 However, SSWs in 2007 and 2010 are included in the regression analysis for Figure 6 for more robust  
 8 statistics which also shows that they had some of the lowest impact on ozone.

9 This study also analyzes the impact of different dynamical transport mechanisms on ozone for  
 10 each of the major SSWs. The zonal mean tracer concentration is a balance between transport processes  
 11 and the chemical sources and sinks as shown in the continuity equation of the Transformed Eulerian  
 12 Mean (TEM) (Andrews et al, 1987):

$$13 \quad \bar{x}_t = -\bar{v}^* \bar{x}_y - \bar{w}^* \bar{x}_z + e^{z/H} \nabla \cdot M + P - L \quad (2)$$

14 where  $\bar{x}_t$  is the tracer tendency (in this case, ozone mixing ratio tendency),  $(\bar{v}^*, \bar{w}^*)$  are horizontal  
 15 and vertical components of the residual circulation,  $z = -H \ln(p/p_0)$  in log-pressure height using a scale  
 16 height H of 7 km, M is the eddy transport vector, and P and L are chemical production and loss. The  
 17 overbars stand for the zonal average. Subscript symbols denote partial derivatives [with respect to

time (t) and height (z)]. The first two terms on the right-hand side of equation (2) represent the contribution of advective transport on ozone changes. The vertical component of residual circulation is the dominant contributor of advection ( $\bar{w}^*$ ) and can be estimated using TEM (Andrews et al, 1987):

$$\bar{w}^* = \bar{w} + \frac{1}{a \cos \phi(\phi)} \partial_{\phi} (\cos(\phi) \frac{\overline{v' \theta'}}{\theta_z}) \quad (3)$$

where v and w are the meridional and vertical winds,  $\theta$  is potential temperature,  $a$  is the earth radius,  $\phi$  is the latitude. The prime denotes the departure from the zonal mean. The third term on the right side of equation (2) shows the impact of eddy mixing on ozone transport. M can be decomposed into vertical and meridional components  $M_{(z)}$  and  $M_{(y)}$  respectively: (Andrews et al., 1987):

$$M_{(y)} = -e^{(-z/H)} (\overline{v' \chi'} - \frac{\overline{v' \theta'}}{\theta_z} \bar{x}_z) \quad (4)$$

$$M_{(z)} = -e^{(-z/H)} (\overline{w' \chi'} + \frac{\overline{v' \theta'}}{\theta_z} \bar{x}_y) \quad (5)$$

The contribution of dynamical and chemical drivers of ozone anomalies varies throughout the year. During springtime, both dynamical resupply and chemical depletion strongly modulate ozone changes. Assuming an isolated polar vortex and neglecting isentropic mixing, a previous study showed a similar magnitude of influence from chemical ozone depletion processes and dynamical ozone supply during the springtime (Tegtmeier et al. 2008). However, Strahan et al. (2016) used a chemistry and transport model to show that dynamical processing affects ozone changes by a factor of two more than chemical processing during March. However, chemical processes are not significant drivers of ozone changes in the middle stratosphere from November to February in the Arctic because of the polar night (de la Cámara et al. 2018b). Moreover, it has been shown that during years with SSWs, Arctic ozone depletion is significantly diminished (Strahan et al. 2016). However, if prior to or during the SSWs, the polar vortex moves outside of the region of the polar night (to lower latitudes), ozone depletion will occur as shown in the 2013 SSW by Manney et al. (2015). By limiting our analysis to latitudes between 60°N to 80°N, this impact is minimized in our analysis. Because the impact of the chemical components on the evolution of ozone during SSWs is a less important factor below 30 km (de la Cámara et al 2018b), the dynamical analysis in this study will focus on altitudes below 30 km. Thus, neglecting P and L below 30

1 km in further analysis, as chemical production and loss is not an output of reanalysis data, does not lead  
2 to significant non-closure in the presented analysis and does not impact our conclusions. In further  
3 sections, analysis will focus on middle stratospheric layers between 15 and 30 km.

#### 4 **4. Comparison of Observations with MERRA-2**

5 In this section, the results of the comparisons between MERRA-2 and observations from  
6 ozonesondes and FTIR retrievals during SSWs are discussed. Ground-based observations provide an  
7 excellent baseline to assess climate models and assimilated systems. However, the use of ground-based  
8 observations to directly study the impact of SSWs is challenging because of the coarse time resolution of  
9 ozonesondes, limited clear-sky conditions and sunlight for FTIR measurements, and dealing with one  
0 profile per site/launch time for each sensor, and its subjectivity to the site location and time. In this study,  
1 we take advantage of a dense network of observations over the Greenland sector (60°N to 80°N and 10°W  
2 to 70 °W) to assess the performance of MERRA-2 over the high latitudes. The use of MERRA-2 allows  
3 us to investigate the fluctuations over the entire Arctic with consistent temporal and spatial resolution.  
4 To visualize the observation frequency and the overall performance of MERRA-2, the time series of PCO  
5 from MERRA-2 3-hourly data and ozonesondes and FTIR from winter 2007 to spring 2009 are shown in  
6 Figure 2.

7 Two major SSWs occurred during this time period. To exhibit a consistent time series and to  
8 avoid the impact of the variability of maximum height of the ozonesondes, PCO from the ground to 20  
9 km is shown. Figure 2 shows the high temporal frequency of the FTIR retrievals compared to  
0 ozonesondes during polar day, the consistent frequency of ozonesondes throughout the year, and the gap  
1 in solar FTIR retrievals at high latitudes during polar night. The results indicate a good overall agreement  
2 of MERRA-2 with observations. The sparsity of FTIR ozone retrievals at Thule in 2008 was due to  
3 instrument issues. To have a more clear understanding of the uncertainties in MERRA-2 estimations,  
4 more quantitative comparisons are needed.

5 To investigate the uncertainties of MERRA-2 ozone data during the highly anomalous conditions  
6 during SSWs and to consider the enduring impact of SSWs on trace gases, comparisons are performed  
7 from 1 December to 1 May for all six events. The results and statistics of comparisons between

1 ozonesondes and MERRA-2 are depicted as the relative differences in Figure 3. The PCO relative  
2 difference is estimated as PCO from MERRA-2 minus ozonesonde PCO divided by ozonesonde PCO for  
3 ground to 5km (G-5km), 5km-10km, and 10km-30km. These layers indicate different performances of  
4 MERRA-2 by height and show the effect of atmospheric pressure on the contribution of each level to the  
5 total ozone column. The G-5km layer includes the troposphere, the 5-10km layer includes the upper  
6 troposphere low stratosphere (UTLS), while the 10-30km layer includes the lower and middle  
7 stratosphere. The partial column is calculated only up to the altitude of the balloon burst of the  
8 ozonesonde, if the burst height is below 30 km.

9 Large relative differences between MERRA-2 and the ozonesondes near the surface indicate a  
0 well-defined high bias in MERRA-2 at Ny-Alesund and Eureka. The occasional extreme low ozone  
1 mixing ratios observed in the lower atmosphere and near the surface are linked to catalytic reactions  
2 involving bromine. This chemical ozone depletion is more common at Arctic sites near the ocean  
3 (Tarasick and Bottenheim, 2002). The extreme low ozone values near the surface are not represented in  
4 MERRA-2 as it does not include bromine chemistry.

5 Overall, the variability of the relative differences at lower altitudes are larger (Figure 3). Ny-  
6 Alesund and Eureka show 5%(±23%) and 18%(±26%) mean (±std) difference ratio at G-5km. However,  
7 the G-5km layer, on average, contains less than 20 DU, which is less than 6% of total column ozone  
8 (TCO). PCO of the G-5 km layer is only 1.5% of TCO at Summit Station where the site elevation is 3.2  
9 km. The PCO difference ratio at Summit station shows very small bias with a standard deviation of ±15%.

10 The positive bias decreases higher in the troposphere, and the scatter plot shows negative relative  
11 differences. From 5 km to 10 km, a negative mean bias exists at all sites however they are accompanied  
12 by a larger the standard deviation. The mean PCO relative differences from 5 km to 10km are -8%(±13%),  
13 -15%(±15%), and -8%(±16%) at Summit Station, Ny-Alesund, and Eureka.

14 The MERRA-2 ozone data between 10 and 30 km are highly correlated with the ozonesondes  
15 with  $R^2 > 90\%$  (not shown). From 10 to 15 km, the relative differences are slightly positive and, above  
16 15 km, a negligible bias and low standard deviations are observed. The mean PCO difference ratio in the  
17 10-30 km layer is equal to or less than 3% (±7%) at all stations. The differences between 10 and 30 km

1 are more impactful in TCO uncertainty analysis because this region contributes most to the total column  
2 ozone. (The average PCO for each layer is reported in Figure 3.)

3 Figure 4 summarizes the comparison between the MERRA-2 and the FTIR retrievals for  
4 December 1st to May 1st for all six SSW years. The partial column comparisons for ground to 8 km, 8-  
5 15 km, 15-22 km, and 22-34 km are shown. Here the partial columns are defined based on the averaging  
6 kernel of the NDACC retrievals. The mean and standard deviation of relative differences, and the mean  
7 PCO for each layer are shown in Figure 4.

8 The layers between 15-22 km and 22-34 km contain the most column ozone with averages of 146  
9 DU and 101 DU, respectively. MERRA-2 and the FTIR retrievals have good agreement in these layers  
0 with relative differences of  $-2\% \pm 5\%$  and  $-4\% \pm 5\%$ , respectively.

1 In the lowest layer, the differences are the largest with a standard deviation ratio of higher than  
2 15% at all stations and mean differences in the range of  $-7\%$  to  $3\%$ . Large differences are observed  
3 between 8-15 km, where MERRA-2 estimates  $7\%$ - $13\%$  more ozone than the FTIR retrievals, and the  
4 standard deviations are large. Large differences and standard deviations below 15 km indicate that higher  
5 uncertainties exist in both the FTIR retrievals and the MERRA-2 estimation

6 In conclusion, when compared to observations, MERRA-2 captures large fluctuations in middle  
7 stratospheric ozone at high northern latitudes during winters and early spring that are impacted by SSWs.  
8 The agreement between MERRA-2 ozone with observations during SSWs motivates the use of MERRA-  
9 2 dataset to further understand mid-stratospheric ozone fluctuations during SSWs. The differences in the  
10 lower stratospheric and tropospheric layers exhibit larger values. The higher uncertainties below 10 km  
11 during the five months impacted by SSWs are consistent with higher uncertainties in MERRA-2 in these  
12 layers year-round, as seen in previous studies (Gelaro et al., 2017; Wargan et al., 2017). However, still  
13 large fluctuations of lower atmosphere ozone are discernible from MERRA-2 data (Knowland et al. 2017;  
14 Jaeglé et al. (2017); Albers et al, 2018). The maximum height of ozonesondes is around 30-35 km and  
15 ground-based remote sensing loses sensitivity with increasing altitude, thus this study cannot improve  
16 previous research on the upper stratosphere where higher uncertainties were reported compared to the  
17 mid stratosphere. Because more than 80% of ozone molecules exist in the middle stratosphere (15 to 30

1 km), the total column uncertainty is dominated by uncertainties in mid-stratospheric layers. In the  
2 following section, we discuss ozone variability in the total column and the vertical profile up to 60 km,  
3 while our primary analysis is focused on ozone and dynamical processes the mid-stratospheric layers,  
4 which contribute most to the TCO and where the measurements are most reliable.

## 5 **5. SSWs and their impact on ozone**

6 Disturbances in stratospheric circulation have an impact on stratospheric trace gas concentrations.  
7 Consequently, the temporal changes of trace gas concentrations can provide a better understanding of  
8 atmospheric circulation including vertical and horizontal transport (Manney et al., 2009a). In this section,  
9 the impact of altered circulation patterns on ozone is analyzed, and by investigating the evolution of the  
0 polar vortex and temperature more detailed characterization of ozone variability is provided.

1 To understand the alteration of ozone and the average position of the polar vortex before and after  
2 each SSW, the anomaly of total column ozone (TCO) and the average Ertel's potential vorticity (PV) are  
3 investigated. The anomaly of TCO average and PV average for 15 days preceding and 15 days after each  
4 of the SSWs are shown in Figure 5. The TCO anomaly is calculated using a climatology based on the  
5 same days of averaged non-SSW years since 2004. PV contours of 600 and 800 ( $10^{-6} \text{ K m}^2 \text{ Kg}^{-1} \text{ s}^{-1}$ ) at  
6 isentropic level with the potential temperature of 850 K ( $\sim 30$  km) indicate the dominant area of the polar  
7 vortex. In the following section the main characterization of each SSW, the evolution of the polar vortex,  
8 and TCO changes are discussed.

9 2006: On 21 January 2006, the second strongest and prolonged major SSW since 2004 was  
10 detected (Table II, Siskind et al., 2007; Manney et al., 2008b; 2009a). The easterly zonal mean zonal  
11 wind lasted 26 days. Prior to the major SSW, a minor SSW was detected on 9 January (Manney:2008b,  
12 Manney:2009a). The polar vortex moved toward Siberia and receded away from Greenland during the  
13 minor warming. The polar vortex then displaced westward and equatorward toward northwestern Europe  
14 before the major SSW as shown in Figure 5a1.

15 2008: The dynamical circulation was quite variable during winter 2008. Two minor SSWs in mid  
16 and late January and one major SSW in late-February are recorded in 2008 (Goncharenko and Zhang,

1 2008; Flury et al., 2009; Thurairajah et al., 2010; Korenkov et al., 2012). The easterly winds lasted 16  
2 days after the major warming on 22 February. This event is recorded as the latest in the winter season  
3 and the least prolonged among the six SSWs considered in this study (Table II). The polar vortex is  
4 displaced mostly over northwest Europe during the development of the SSW in 2008 as shown in Figure  
5 5b1. The polar vortex displacement over Europe led to ozone depletion and the enhancement of  
6 stratospheric water vapor over northern Europe by mid-February (Flury et al, 2009).

7 2009: Following an undisturbed and cold early winter, the strongest and most persistent SSW  
8 among this study's events occurred on 2 January 2009 as shown in Table II (Manney et al., 2009b; Harada  
9 et al., 2010; Lee and Butler, 2019). The extended elongated shape of the polar vortex before the SSW can  
0 be seen in Figure 5c1, which was followed by a split vortex. The prolonged SSW in late January recorded  
1 30 days of easterlies at 10 hPa with a maximum magnitude of 29 m/s (Table II).

2 2013: The atmospheric disruption associated with the major SSW on 6 January 2013 displaced  
3 the polar vortex toward Europe (Figure 5d1) and eventually split the stratospheric polar vortex into  
4 smaller vortices over Canada and Siberia in mid to late January (Manney et al., 2015). The isolated,  
5 offspring vortex over Canada lasted for more than two weeks as shown in Figure 5d2.

6 2018: A major SSW was detected on 12 February 2018. However, the disturbed circulation started  
7 in January, with 8 days of zonal wind deceleration occurring in mid-January (Rao et al., 2018). The  
8 elongated pattern of PV from Europe to eastern Canada shown in Figure 5e1 indicates a highly disturbed  
9 vortex prior to the major SSW resulting in a vortex split (Karpechko et al., 2018; Rao et al., 2018; Butler  
0 et al. 2020). The split vortices were located over Canada/northwest US and northwestern Europe and  
1 lasted for almost a week after the detected SSW. The signal of the offspring vortex after the SSW event  
2 over Canada is visible in Figure 5e2. The major SSW caused record-breaking cold surface temperatures  
3 in northwest Europe (Greening and Hodgson, 2019).

4 2019: The major SSW on 2 January 2019 (Butler et al. 2020; Rao et al., 2019, Schranz et al.,  
5 2020) is the earliest in the winter season and weakest in magnitude of reversal among the most recent six  
6 events studied here (Table II). The polar vortex was displaced towards Europe before the major SSW  
7 occurred (Figure 5f1). The continuous wave activity caused a vortex displacement to be followed by a



1 split vortex. The resulting vortices were located over the northeastern US and northwestern Europe as  
2 shown in Figure 5f2.

3 As shown in Figure 5, the averaged vortex displacement occurs towards the southeast (Europe)  
4 prior to the major SSW as seen in 2006, 2008, 2013, and 2019 (hereafter the displaced vortex SSWs),  
5 and is accompanied by an early positive ozone anomaly in the region outside of the vortex which includes  
6 parts or all of the north pole, high latitude North America, eastern Siberia, and the Greenland sector. After  
7 the vortex breakdown, the geographical extent of the positive ozone anomalies is mostly limited to high  
8 latitudes with a fairly symmetrical shape around the Arctic in these cases. On the other hand, an elongated  
9 averaged polar vortex prior to the major SSW as seen in 2009 and 2018 (hereafter the elongated vortex  
0 SSWs) is associated with negative ozone anomalies over a large extent of high latitudes, followed by  
1 strongly positive TCO anomalies over an extensive area after vortex breakdown.

2 The averaged polar vortex state we refer to in this study is different, though often related to, split  
3 and displaced vortex morphology discussed in previous literature (e.g., Charlton and Polvani 2007). As  
4 seen during the SSWs in 2018 and 2009, in which the polar vortex split, the 15-day average polar vortex  
5 before those events is elongated. Other events, such as those in 2013 and 2019, first displace and then  
6 split. However, here we consider them displaced SSWs if the 15-day average EPV prior to the event is  
7 displaced and not elongated. Previous studies focused on the connection of the type of polar vortex  
8 breakdown to its impact on the speed of trace gas transitions (Charlton & Polvani (2007); Manney et al.  
9 2009b). This study investigates the modulation of the magnitude and extent of ozone changes, and the  
10 results show that the average EPV shape before the vortex breakdown is more influential than the final  
11 form of polar vortex breakdown.

12 To investigate the connection of polar vortex strength and TCO, the scatter plot of the zonally  
13 averaged (60°N to 80°N) EPV change at the potential temperature of 850 K versus the corresponding  
14 change in TCO (60°N to 80°N) is shown in Figure 6. All averages are area weighted, and the ratio of  
15 change for each variable is estimated as the average of 15 days after SSWs subtracted by the average of  
16 15 days before the SSWs and divided by the average of 15 days before the SSWs. To increase the  
17 robustness of regression analysis, SSWs in 2007 and 2010 are also included here (Fig. 6). The correlation

1 between the magnitude of change in EPV and TCO is very strong ( $R^2= 90\%$ ). The elongated vortex  
2 SSWs (2009 and 2018) exhibit a higher magnitude of change in both EPV and TCO in this period. This  
3 result shows that the averaged polar vortex shape before the SSWs is connected to the EPV change and  
4 then dramatically influences the magnitude of ozone changes at high latitudes.

5 As the Greenland sector is one of the critical regions that is climatologically isolated by the polar  
6 vortex, the variability of area-weighted ozone average over the Greenland sector ( $60^\circ\text{N}$  to  $80^\circ\text{N}$  and  $10^\circ\text{W}$   
7 to  $70^\circ\text{W}$ ) as well as the zonal average ( $60^\circ\text{N}$  to  $80^\circ\text{N}$ ) is analyzed to investigate the similarities and  
8 differences of the impacts of SSWs on zonal and regional high latitude ozone. The structure of ozone  
9 anomalies in the zonal minus Greenland sector is similar to the zonal average. The Greenland sector has  
0 been shown to be uniquely sensitive to dynamical forcing associated with the Quasi-Biennial Oscillation  
1 (QBO) (Anstey and Shepherd, 2014; Bahramvash-Shams et al., 2019). Moreover, the air masses above  
2 the Greenland sector are more strongly isolated than at other Arctic longitudes during wintertime, as  
3 shown by the climatology of the polar vortex and its associated minimum temperature in Figure 1. Thus,  
4 it is important to understand the regional impact of SSWs on the Greenland sector.

5 To track the strength of the polar vortex, the area-weighted average of PV at the potential  
6 temperature of 850 K over the zonal average ( $60^\circ\text{N}$ - $80^\circ\text{N}$ ) and the Greenland sector ( $60^\circ\text{N}$ - $80^\circ\text{N}$ ,  $10^\circ\text{W}$ -  
7  $70^\circ\text{W}$ ) from 40 days before to 60 days after each SSW is shown in the first column of Figure 7. The  
8 evolution of the area-weighted average of TCO for the zonal average and the Greenland sector is shown  
9 in the second column of Figure 7. The climatologies of PV and TCO for both the zonal average and  
10 Greenland sectors in Figure 7 are estimated based on non-SSW years between 2004 to 2019. To quantify  
11 the influence of SSWs on ozone, the average TCO for the period spanning 40 days before to 60 days after  
12 the SSWs is shown in the bottom right of each plot, as well as the ratio of the changes.

13 The Greenland Sector is located inside the climatological polar vortex area (Figure 1) which  
14 explains the higher intensity of climatological EPV over the Greenland sector compared to the zonal  
15 climatology in Figure 7. The impact of minor SSWs in 2006 (around lag -25 and -19) and in 2008 (lag -  
16 30 and -15), as well as sudden polar vortex displacement to Eurasia in 2019 (lag -20) showed a stronger  
17 signal on the averaged EPV over the Greenland sector with a larger drop in EPV in this region compared

1 to the zonal mean. The duration of the polar vortex recovery is defined by the number of days between  
2 the date of the SSW and the date in which the zonal EPV returns to its climatological value, as reported  
3 in the last column of Table II. The fastest recovery of 30 days is observed in 2019 (also the least minimum  
4 easterly value the study's SSWs) and the longest recovery duration of around 45 days is observed in  
5 2009, 2013, and 2018. The recovery duration is similar with only a few days difference if the EPV over  
6 the Greenland sector is used instead.

7 Compared to the 40-day average of TCO prior to the SSW, the highest percent zonal TCO increase  
8 of 29% is observed for one of the elongated polar vortex SSWs in 2009. The relative increase in TCO  
9 over the Greenland sector (blue line) is higher compared to the zonal average (orange line). The  
0 Greenland sector is climatologically inside the polar vortex area and has a lower TCO value during strong  
1 polar vortex which consequently exhibits higher relative increase after the vortex break down and mixing.  
2 However, dynamically disturbed winters such as years with minor SSWs before the major SSWs hinder  
3 the higher relative TCO increase over the Greenland sector compared to the zonal average. For instance,  
4 in 2006, the polar vortex weakened around 25 days before the major SSW (first column Figure 7, TCO  
5 2006) due to a minor SSW, which coincides with the averaged TCO (solid line) increase compared to the  
6 climatology (dashed line) as seen in the second column Figure 7 (TCO 2006). The earlier timing of the  
7 positive anomaly caused a lower value in the TCO change after the event. The relative TCO increase over  
8 the Greenland sector exhibits a higher value during elongated polar vortex SSWs with 37% in 2018 and  
9 31% in 2009. More details of physical mechanisms that cause variability in ozone during SSWs is  
10 discussed in section 6.

11 Analyzing the vertical structure of ozone provides more details of the impact of SSWs. Figure 8  
12 shows the temporal evolution of the vertical structure of ozone as a cross-section of area-weighted ozone  
13 anomalies for both the zonal average (60°N to 80°N) and the Greenland sector from 40 days before to 60  
14 days after each SSW. The anomalies are estimated with respect to the climatology of non-SSW years  
15 between 2004 to 2019. The positive ozone anomaly in mid stratospheric layers (15 to 30km) starts a few  
16 weeks (15 to 25 days) prior to the displaced vortex SSWs (2006, 2008, 2013, and 2019) over both the  
17 zonal average and the Greenland sector. The negative ozone anomalies 15 days before the SSWs and  
18 extreme positive ozone after the SSWs in mid stratospheric layers for the two elongated vortex SSWs

(2009, 2018) are evident. The enduring impact of SSWs on ozone in different atmospheric layers is clear in all cases and shows a similar pattern for both the zonal averaged and the Greenland sector. As expected, the structures of ozone anomalies are smoother in the zonal average compared to the Greenland sector. The impact on ozone with the shortest duration occurred in 2008, which has multiple disturbances in the circulation and the shortest duration of easterlies (Table II).

To highlight the temperature variation, Figure 9 shows the cross-section of the temperature anomaly for the zonal average from 40 days before to 60 days after each SSW. Figure 9 focuses only on the zonal average, as the anomaly of temperature profile had similar patterns over the zonal and the Greenland sectors. The positive temperature anomalies in mid stratospheric layers start a few weeks before the SSWs in the 4 cases of a displaced vortex (2006, 2008, 2013, and 2019). On the other hand, the intrusion of the positive temperature anomalies to mid stratospheric layers is almost coincident with SSWs in the 2 elongated vortex cases. The gradual temperature increases in displaced SSWs point to a buildup of wave forcing in these cases compared to elongated cases. The next section provides more detailed discussion of dynamical mechanisms related to stratospheric ozone changes during SSWs. The duration of positive temperature anomalies in mid stratospheric layers is 10 days to 30 days shorter than ozone positive anomalies (Figure 8 and Figure 9). The positive temperature anomaly is more persistent at lower levels of the stratosphere, where the enduring impact of SSWs on mid-stratosphere ozone (up to 25 -30 km) is clear in all of the SSWs studied here.

## 6. Discussion

The cyclonic polar vortex during wintertime is generated in response to the seasonality of radiative cooling. The intensified wave forcing before the SSW is manifested by both accelerated tropical upwelling and polar downwelling, and by poleward transport of low EPV air parcels. The conservation of EPV causes anticyclonic circulation, which gradually drives easterly zonal mean zonal winds, and leads to the displacement or splitting of the polar vortex. The resultant reduction in the vorticity induces strong descent and consequently an adiabatic temperature increase in the stratosphere (Matsuno, 1971; Limpasuvan et al., 2012).

Here the MERRA-2 dataset is used to determine the impact of the dynamical terms on ozone

1 changes during each SSW. Because of the constraints in tracer continuity estimation using equation (2),  
 2 these analyses are estimated over the Arctic zonal average only and not the Greenland sector. The vertical  
 3 component of the residual circulation ( $\bar{w}^*$ ) as defined in equation (3) is an indicator of wave forcing. The  
 4 cross-section of the vertical component of residual circulation during 40 days prior to and 60 days after  
 5 the SSW over the zonal average (60°N to 80°N) is shown in Figure 10. More intense downward  
 6 propagation is shown as darker blue. The increased wave forcing preceding the SSW is evident in Figure  
 7 10 with negative  $\bar{w}^*$  anomalies, which indicate strong downwelling in the zonal average. Occurrences  
 8 of minor SSWs can be seen through the early appearance of increased wave forcing, as seen in 2006 and  
 9 2008. A very intense and abrupt increase in downward propagation was observed in 2009. Disturbed  
 0 circulations in the middle stratosphere before the SSWs are seen in 2018 and 2019 (lag -30 to -20).

1 Following the SSW, residual circulation is weakened as shown in Figure 10. The intensity of  
 2 increased wave activity is reduced shortly after the SSW. However, the decrease in wave activity is  
 3 gradual, in general, and lasts a few weeks as shown in Figure 10. The suppressed wave activity allows  
 4 for the recovery of the zonal mean zonal wind, temperature, and ozone. Shortly after the SSW, the  
 5 recovery starts in the upper stratosphere as shown in Figure 9. However, different radiative relaxation  
 6 time scales cause a slower recovery in the lower stratosphere compared to upper stratospheric layers  
 7 (Dickinson, 1973; Randel et al., 2002; Hitchcock and Simpson, 2014). The dynamical alteration  
 8 suppresses any further upward propagation of the planetary waves, which explains the descending pattern  
 9 of temperature up to weeks after the SSW (Matsuno, 1971).

10 The impact of each term in tracer continuity (equation (2)) on ozone for each SSW is investigated  
 11 and shown in Figure 11. The composite effect of chemistry during SSWs is important in the upper  
 12 stratosphere (de la Cámara et al 2018b). The analysis of dynamical parameters in this study is limited to  
 13 30 km to minimize the impact of chemical processes. Considering the larger uncertainties of ozone  
 14 estimation in MERRA-2 below 15 km, and the possibility of larger uncertainties in dynamic parameter  
 15 estimations, this study focuses on the impact of dynamical mechanisms on the middle stratospheric (15  
 16 km-30 km) ozone. The cross-section of ozone tendency ( $dO_3/dt$ , left side of equation (2)), the horizontal  
 17 component of eddy mixing  $e^{(z/H)}(a \cdot \cos\phi)^{-1} (\partial(\cos\phi M_{(y)}) / \partial y)$  ( $M_{(y)}$  as defined in equation(4) ), the vertical  
 18 component of eddy mixing  $e^{(z/H)}(\partial M_{(z)} / \partial z)$  ( $M_{(z)}$  as defined in equation(5) ), the horizontal advection

1 transport (the first term on the right side of equation (2)), vertical advection transport (the second term  
2 on the right side of equation (2)), and summation of right side equation(2) (called the estimated ozone  
3 tendency) during the 40 days prior to and 60 days after the SSW over the zonal average are shown in  
4 Figure 11.

5 The estimated ozone tendency (last column of Figure 11) shows that using MERRA-2 fields,  
6 dynamical terms of tracer continuity can simulate the main features of the observed ozone tendency (first  
7 column of Figure 11) from 15 km to 30 km. We use these estimates to investigate the impact of different  
8 terms of tracer continuity on ozone. The key role of vertical advection and horizontal eddy mixing on  
9 ozone tendency is evident in Figure 11. Vertical advection is the main driver of ozone tendency in the  
0 mid stratosphere. Intensified residual circulation (Figure 10) dramatically impacts the ozone increase. A  
1 significant signal of vertical advection is evident from 15 to 30 km in all six SSWs and is coincident with  
2 enhanced wave activity (Figure 10), which is magnified around SSWs; however, it persists well after the  
3 vertical residual circulation signal disappears, up to two months after the SSWs. The sudden and  
4 intensified vertical advection is more magnified in 2009 and 2018 with an enduring elongated polar  
5 vortex.

6 Horizontal eddy mixing is the second important contributor in ozone tendency over the mid  
7 stratosphere. While vertical advection builds up the ozone tendency, horizontal mixing tends to balance  
8 and weaken the ozone tendency. Increased wave activity and large-scale mixing drive a prolonged  
9 enhancement of the diffusivity of PV flux, which leads to increased horizontal eddy transport (Nakamura,  
10 1996; de la Cámara et al., 2018a; 2018b). Vertical eddy mixing has a clear signal above 20 km during  
11 minor and major SSWs. Horizontal advection has the least significant contribution to ozone tendency.  
12 The dominant contribution of vertical advection on mid-stratospheric ozone variability (15 to 30 km)  
13 using MERRA-2 dynamic parameters is consistent with climate model analysis (Tao et al., 2015; de la  
14 Cámara et al., 2018b). This study shows that the larger geographical extent and magnitude of ozone  
15 changes during SSWs with elongated polar vortex is tied to greater vertical advection during these events.

16 The time series of vertically integrated (15 to 30 km) ozone tendency, horizontal eddy mixing,  
17 vertical advection, and the residual of tracer continuity considering all terms in equation (2) are shown in

1 Figure 12. The major contribution of vertical advection on ozone tendency is evident in Figure 12. The  
2 higher intensity of ozone tendency and vertical advection and their strong correlation coincident with the  
3 SSW date of the elongated polar vortex (2009 and 2018) stand out.

4 Although the estimated ozone tendency (last column in Figure 11) simulates most features of the  
5 observed ozone tendency (the first column in Figure 11), they are not identical. The vertically integrated  
6 difference in observed and estimated ozone tendency is shown as the residual. The residual of tracer  
7 continuity results from both the numerical approximation of terms in equation (2) (errors in the horizontal  
8 derivatives over high latitude can be large as  $\cos(\varphi)$  gets small) as well as the uncertainties in the balance  
9 of dynamical parameters in the reanalysis due to the data assimilation process (Martineau et al. 2018).  
0 Also, the possibility of chemical processes during splitting or displacement of the polar vortex out of the  
1 polar night region might contribute to the residual of tracer continuity. It should be noted that when  
2 viewing individual events, the plots are expected to be noisier than the average of numerous events.

### 3 **7. Summary and Conclusion**

4 SSWs are a major manifestation of disturbed stratospheric circulations. The altered dynamics  
5 influence the cycle of trace gases including ozone. The MERRA-2 reanalysis is used to investigate the  
6 influence of six persistent SSWs from 2004 to 2020 on ozone for the zonal average at high latitudes (60°N  
7 to 80°N). The variability in impact of SSW on high latitude ozone is analyzed, two different patterns are  
8 found, and possible related dynamical mechanisms are studied.

9 The comparison of the MERRA-2 ozone dataset with a unique density of observations at high  
10 latitudes provides an update to previous evaluations and provides understanding of the performance of  
11 MERRA-2 during high variability associated with extreme dynamical events such as SSWs. Comparisons  
12 are applied during December to May for each SSW. MERRA-2 shows good agreement with ozonesondes  
13 and FTIR observations in the middle stratosphere during highly altered dynamics of SSWs.

14 Comparison with ozonesondes at three high latitude locations showed the mean difference ratio  
15 of 3% ( $\pm 7\%$ ) in the stratosphere layer (10-30 km). However, the uncertainties are larger from the ground  
16 to 10 km. From 5km to 10km, negative mean bias exists in all sites (-8% to 15%) however, it is

1 accompanied by a large standard deviation. Around 20% standard deviation of relative differences is  
2 observed at G-5 km. A positive bias is observed at surface levels where observations show depleted ozone  
3 due to bromine reactions.

4 Using a smoothing method, MERRA-2 is compared to five NDACC FTIR sites in four vertical  
5 layers (ground-8km, 8-15km, 15-22km, and 22-30km) during SSWs. These layers are defined based on  
6 the sensitivity of FTIR sensors. Overall, higher uncertainties are observed at the lowest level with 18%  
7 std. The best agreement is observed between 15-22 km and 22-34 km with  $-2\%(\pm 5\%)$  and  $-4\%(\pm 5\%)$   
8 mean(std) relative differences. These results emphasize the high quality of MERRA-2 after August 2004,  
9 when MLS data is available, and motivate its usage in mid stratospheric ozone analysis at high northern  
0 latitudes during highly disturbed dynamical events. Higher uncertainties in UTLS are also expected  
1 because MLS is a dominant contribution in MERRA-2 ozone profiles and has lower sensitivity at lower  
2 altitudes. Moreover, this study emphasizes the importance of independent ozone observations, such as  
3 ozonesondes and FTIR retrievals, as a means to evaluate models and assimilation estimations around the  
4 globe.

5 Using the MERRA-2 dataset, the variability of ozone changes during the SSWs and associated  
6 dynamic parameters are investigated. The evolution of the polar vortex and its impact on the ozone  
7 variability is studied using the average EPV at the potential temperature of 850 K. We identify two  
8 different patterns in the averaged polar vortex before the SSWs and the subsequent impact on ozone. In  
9 2009 and 2018, an elongated polar vortex is observed before the SSWs which caused a predominantly-  
10 negative ozone anomaly at northern high latitudes and is followed by an extensive positive ozone  
11 anomaly with large geographical extent. The TCO increase rates and the magnitude of changes in EPV  
12 after these cases are large and the intrusion of positive temperature anomalies to the mid stratosphere is  
13 coincident with these SSWs dates.

14 During the SSWs in 2006, 2008, 2013, and 2019, the averaged polar vortex is displaced towards  
15 Europe, and the TCO exhibits positive anomalies before the SSWs in a large geographical region of  
16 northern high latitudes (outside the polar vortex). The positive TCO anomalies after the SSW have a  
17 smaller extent, and the magnitude of TCO variability and EPV change is smaller compared to observed



1 changes during the elongated vortex events in 2009 and 2018. During these displaced events, the positive  
2 temperature anomalies in the middle stratosphere appear a few weeks before the SSW.

3 A strong correlation of  $R^2= 90\%$  is observed between the magnitude of change in the averaged  
4 EPV around the SSW and the magnitude of TCO change for the same period for all six studied SSWs  
5 plus two less persistent SSWs in 2007 and 2010. The regression analysis also emphasized the larger  
6 changes in both EPV and TCO during elongated SSWs.

7 The Greenland sector is one of the critical regions that is impacted by negative TCO anomalies  
8 before the elongated polar vortex in 2009 and 2018; positive TCO anomalies occur before displaced  
9 SSWs. To identify the similarities and differences of zonal versus the regional impact of SSWs on ozone,  
0 the analyses are applied over the Greenland sector as well as the zonal average. The general structure of  
1 the vertical ozone anomaly over the Greenland sector is similar to the zonal structure. However, as  
2 expected the ozone anomaly over the zonal average is smoother than the Greenland sector which results  
3 in a more magnified TCO increase over Greenland. The increased rate over the Greenland sector is  
4 between 15% in 2006 to 38% in 2018, while the zonal average ranges between 8% in 2008 to 29% in  
5 2009.

6 We examined the dynamical terms associated with ozone tendency and investigated the evolution  
7 of ozone variability for each SSW using MERRA-2. The main features of observed mid stratospheric  
8 ozone tendency are captured by the dynamical terms of the tracer continuity equation using MERRA-2  
9 variables. Vertical advection is shown to be the main contributor of ozone tendency in the middle  
10 stratosphere during the SSWs and is more magnified during the enduring elongated polar vortex in 2009  
11 and 2018. The impact of vertical advection coincides with the time of enhanced wave activity but can  
12 persist up to two months after the SSWs.

13 Suppressed wave activity initiates the recovery of temperature and ozone. However, the upper  
14 stratosphere experiences a faster recovery compared to the lower stratosphere because of the different  
15 radiative relaxation time scales (Randel et al., 2002). The fastest recovery of zonally averaged  
16 temperature and ozone at the middle stratosphere happen in 30 days for 2008. The positive ozone anomaly  
17 in the middle stratosphere lasts longer than the positive temperature anomaly in most of the SSWs by 10

1 days or more.

2 In conclusion, the MERRA-2 dataset is shown to capture the ozone variability in the middle  
3 stratosphere and provides dynamical information to investigate the impact of SSWs. This study shows  
4 that the averaged vortex shape before the SSWs is an important modulator of the magnitude and extent  
5 of ozone changes over high latitudes. The impact of SSWs on ozone is shown to be more intense in 2009  
6 and 2018 with an elongated polar vortex compared to the displaced vortices in 2006, 2008, 2013, and  
7 2019. The magnitude of change in ozone is correlated with the magnitude of EPV change during the  
8 SSWs. The intensified vertical advection and abrupt wave forcing in during elongated vortex events is  
9 tied to the more intense magnitude and larger geographical extent of ozone changes during these events.  
0 The addition of future SSW events could help to shed light on further details and to create more robust  
1 statistics regarding Arctic SSWs. Although there is no consensus across future climate simulations on  
2 whether SSW occurrences will increase or decrease in response to increased greenhouse gas  
3 concentration (Ayarzarguena et al. 2018, 2020), many simulations show a significant change. The  
4 dramatic ozone increases over high latitudes during SSWs points to the consequences and implications  
5 for ozone if the rate of SSW increases in future.

## 6 **Acknowledgements**

7 We acknowledge NASA's Global Monitoring and Assimilation Office (GMAO) for providing  
8 the Modern-Era Retrospective analysis for Research and Applications, Version 2 (MERRA-2). We  
9 acknowledge the Ozone and Water Vapor Group at the Earth System Research Laboratory of the National  
10 Oceanic and Atmospheric Administration for use of the ozonesonde data and the science technicians at  
11 Summit Station, Greenland for launching the ozonesondes. We acknowledge World Ozone and  
12 Ultraviolet Radiation Data Centre (WOUDC) for providing Canadian and Norwegian ozonesondes. We  
13 acknowledge the Network for the Detection of Atmospheric Composition Change (NDACC) for  
14 providing trace gas retrievals from solar FTIRs. This research was supported by NSF grants PLR-  
15 1420932 and PLR-1414314.

## 16 **References**

- 1 Albers, J. R., Perlwitz, J., Butler, A. H., Birner, T., Kiladis, G. N., Lawrence, Z. D., Manney, G. L., Langford,  
2 A. O., and Dias, J.: Mechanisms Governing Interannual Variability of Stratosphere-to-Troposphere  
3 Ozone Transport, *J. Geophys. Res.*, 123, 234–260, <https://doi.org/10.1002/2017jd026890>, 2018.
- 4 Ancellet, G., Daskalakis, N., Raut, J. C., Tarasick, D., Hair, J., Quennehen, B., Ravetta, F., Schlager, H.,  
5 Weinheimer, A. J., Thompson, A. M., Johnson, B., Thomas, J. L., and Law, K. S.: Analysis of the  
6 latitudinal variability of tropospheric ozone in the Arctic using the large number of aircraft and  
7 ozonesonde observations in early summer 2008, *Atmos. Chem. Phys.*, 16, 13341–13358,  
8 <https://doi.org/10.5194/acp-16-13341-2016>, 2016.
- 9 Andrews, D. G., Holton, J. R., and Leovy, C. B.: *Middle atmosphere dynamics*, Academic Press, 1987.
- 0 Anstey, J. A. and Shepherd, T. G.: High-latitude influence of the quasi-biennial oscillation, *Q. J. R. Meteorol.*  
1 *Soc.*, 1, 1–21, <https://doi.org/10.1002/qj.2132>, 2014.
- 2 Ayarzagüena, B., Polvani, L. M., Langematz, U., Akiyoshi, H., Bekki, S., Butchart, N., Dameris, M., Deushi,  
3 M., Hardiman, S. C., Jöckel, P., Klekociuk, A., Marchand, M., Michou, M., Morgenstern, O.,  
4 O'Connor, F. M., Oman, L. D., Plummer, D. A., Revell, L., Rozanov, E., Saint-Martin, D., Scinocca,  
5 J., Stenke, A., Stone, K., Yamashita, Y., Yoshida, K., and Zeng, G.: No robust evidence of future  
6 changes in major stratospheric sudden warmings: a multi-model assessment from CCMI, *Atmos.*  
7 *Chem. Phys.*, 18, 11277–11287, <https://doi.org/10.5194/acp-18-11277-2018>, 2018.
- 8 Ayarzagüena, B., Charlton-Perez, A. J., Butler, A. H., Hitchcock, P., Simpson, I. R., Polvani, L. M., Butchart,  
9 N., Gerber, E. P., Gray, L., Hassler, B., Lin, P., Lott, F., Manzini, E., Mizuta, R., Orbe, C., Osprey,  
10 S., Saint-Martin, D., Sigmond, M., Taguchi, M., Volodin, E. M., and Watanabe, S.: Uncertainty in  
11 the Response of Sudden Stratospheric Warmings and Stratosphere-Troposphere Coupling to  
12 Quadrupled CO<sub>2</sub> Concentrations in CMIP6 Models, *J Geophys. Res. Atmo.*, 125,  
13 <https://doi.org/10.1029/2019jd032345>, 2020.
- 14 Bahramvash-Shams, S., Walden, V. P., Petropavlovskikh, I., Tarasick, D., Kivi, R., Oltmans, S., Johnson, B.,  
15 Cullis, P., Sterling, C. W., Thölix, L., and Errera, Q.: Variations in the vertical profile of ozone at  
16 four high-latitude Arctic sites from 2005 to 2017, *Atmos. Chem. Phys.*, 19, 9733–9751,  
17 <https://doi.org/10.5194/acp-19-9733-2019>, 2019.
- 18 Baldwin, M. P. and Dunkerton, T. J.: Stratospheric Harbingers of Anomalous Weather Regimes, *Science*, 294,  
19 581–584, <https://doi.org/10.1126/science.1063315>, 2001.
- 20 Baldwin, M. P., Ayarzagüena, B., Birner, T., Butchart, N., Butler, A. H., Charlton-Perez, A. J., Domeisen, D.  
21 I. V., Garfinkel, C. I., Garny, H., Gerber, E. P., Hegglin, M. I., Langematz, U., and Pedatella, N. M.:  
22 Sudden Stratospheric Warmings, *Rev. Geophys.*, 59, 27.1-37, <https://doi.org/10.1029/2020rg000708>,

2021.

- 2 Bevis, M., Harig, C., Khan, S. A., Brown, A., Simons, F. J., Willis, M., Fettweis, X., Broeke, M. R. van den,  
3 Madsen, F. B., Kendrick, E., Caccamise, D. J., Dam, T. van, Knudsen, P., and Nylén, T.: Accelerating  
4 changes in ice mass within Greenland, and the ice sheet's sensitivity to atmospheric forcing, *Proc.*  
5 *Natl. Acad. Sci.*, 1934–1939, <https://doi.org/10.1073/pnas.1806562116>, 2019.
- 6 Bogner, K., Zhao, X., Strong, K., Boone, C. D., Bourassa, A. E., Degenstein, D. A., Drummond, J. R., Duff,  
7 A., Goutail, F., Griffin, D., Jeffery, P. S., Lutsch, E., Manney, G. L., McElroy, C. T., McLinden, C.  
8 A., Millán, L. F., Pazmiño, A., Sioris, C. E., Walker, K. A., and Zou, J.: Updated validation of ACE  
9 and OSIRIS ozone and NO<sub>2</sub> measurements in the Arctic using ground-based instruments at Eureka,  
0 Canada, *J. Quant. Spectrosc. Radiat. Transf.*, 238, 106571,  
1 <https://doi.org/10.1016/j.jqsrt.2019.07.014>, 2019.
- 2 Butler, A. H., Polvani, L. M., and Deser, C.: Separating the stratospheric and tropospheric pathways of El  
3 Niño–Southern Oscillation teleconnections, *Environ. Res. Lett.*, 9, 024014–10,  
4 <https://doi.org/10.1088/1748-9326/9/2/024014>, 2014.
- 5 Butler, A. H., Seidel, D. J., Hardiman, S. C., Butchart, N., Birner, T., and Match, A.: Defining Sudden  
6 Stratospheric Warmings, *Bull. Amer. Meteor. Soc.*, 96, 1913–1928, [https://doi.org/10.1175/bams-d-](https://doi.org/10.1175/bams-d-13-00173.1)  
7 13-00173.1, 2015.
- 8 Butler, A. H., Sjöberg, J. P., Seidel, D. J., and Rosenlof, K. H.: A sudden stratospheric warming compendium,  
9 9, 63–76, <https://doi.org/10.5194/essd-9-63-2017>, 2017.
- 10 Butler, A., Perez, A. C., Domeisen, D. I. V., Garfinkel, C., Gerber, E. P., Hitchcock, P., Karpechko, A. Y.,  
11 Maycock, A. C., Sigmond, M., Simpson, I., and Son, S.-W.: Sub-seasonal Predictability and the  
12 Stratosphere, *Sub-seasonal to Seasonal Prediction*, [https://doi.org/10.1016/b978-0-12-811714-](https://doi.org/10.1016/b978-0-12-811714-9.00011-5)  
13 9.00011-5, 2019.
- 14 Butler, A. H. and Gerber, E. P.: Optimizing the Definition of a Sudden Stratospheric Warming, *J. Climate*, 31,  
15 2337–2344, <https://doi.org/10.1175/jcli-d-17-0648.1>, 2018.
- 16 Butler, A. H., Lawrence, Z. D., Lee, S. H., Lillo, S. P., and Long, C. S.: Differences between the 2018 and  
17 2019 stratospheric polar vortex split events, *Q. J. R. Meteorol. Soc.*, 146, 3503–3521,  
18 <https://doi.org/10.1002/qj.3858>, 2020.
- 19 Cagnazzo, C., and E. Manzini.: Impact of the Stratosphere on the Winter Tropospheric Teleconnections  
20 between ENSO and the North Atlantic and European Region, *J. Climate*, 22(5), 1223–1238,  
21 [doi:10.1175/2008JCLI2549.1](https://doi.org/10.1175/2008JCLI2549.1), 2009.

- 1 Calvo, N., Polvani, L. M., and Solomon, S.: On the surface impact of Arctic stratospheric ozone extremes,  
2 Environ. Res. Lett., 10, 094003–9, <https://doi.org/10.1088/1748-9326/10/9/094003>, 2015.
- 3 Cámara, A. de la, Abalos, M., and Hitchcock, P.: Changes in Stratospheric Transport and Mixing During  
4 Sudden Stratospheric Warmings, J. Geophys. Res., 123, 3356–3373,  
5 <https://doi.org/10.1002/2017jd028007>, 2018a.
- 6 Cámara, A. de la, Abalos, M., Hitchcock, P., Calvo, N., and Garcia, R. R.: Response of Arctic ozone to sudden  
7 stratospheric warmings, Atmos. Chem. Phys., 18, 16499–16513, [https://doi.org/10.5194/acp-18-](https://doi.org/10.5194/acp-18-16499-2018)  
8 16499-2018, 2018b.
- 9 Cámara, A. de la, Birner, T., and Albers, J. R.: Are Sudden Stratospheric Warmings Preceded by Anomalous  
0 Tropospheric Wave Activity?, J. Climate, 32, 7173–7189, <https://doi.org/10.1175/jcli-d-19-0269.1>,  
1 2019.
- 2 Charlton, A. J. and Polvani, L. M.: A New Look at Stratospheric Sudden Warmings. Part I: Climatology and  
3 Modeling Benchmarks, J. Climate, 20, 449–469, <https://doi.org/10.1175/jcli3996.1>, 2007.
- 4 Charlton-Perez, A. J., Ferranti, L., and Lee, R. W.: The influence of the stratospheric state on North Atlantic  
5 weather regimes, Q. J. R. Meteorol. Soc., 144, 1140–1151, <https://doi.org/10.1002/qj.3280>, 2018.
- 6 Coy, L. and Pawson, S.: The Major Stratospheric Sudden Warming of January 2013: Analyses and Forecasts  
7 in the GEOS-5 Data Assimilation System, Mon. Wea. Rev., 143, 491–510,  
8 <https://doi.org/10.1175/mwr-d-14-00023.1>, 2015.
- 9 Coy, L., Eckermann, S., and Hoppel, K.: Planetary Wave Breaking and Tropospheric Forcing as Seen in the  
10 Stratospheric Sudden Warming of 2006, J. Atmos. Sci., 66, 495–507,  
11 <https://doi.org/10.1175/2008jas2784.1>, 2009.
- 12 Coy, L., Wargan, K., Molod, A. M., McCarty, W. R., and Pawson, S.: Structure and Dynamics of the Quasi-  
13 Biennial Oscillation in MERRA-2, J. Climate, 29, 5339–5354, [https://doi.org/10.1175/jcli-d-15-](https://doi.org/10.1175/jcli-d-15-0809.1)  
14 0809.1, 2016.
- 15 Davis, S. M., Hegglin, M. I., Fujiwara, M., Dragani, R., Harada, Y., Kobayashi, C., Long, C., Manney, G.  
16 L., Nash, E. R., Potter, G. L., Tegtmeier, S., Wang, T., Wargan, K., and Wright, J. S.: Assessment  
17 of upper tropospheric and stratospheric water vapor and ozone in reanalyses as part of S-RIP, Atmos.  
18 Chem. Phys., 17, 12743–12778, <https://doi.org/10.5194/acp-17-12743-2017>, 2017.
- 19 Dickinson, R. E.: Method of parameterization for infrared cooling between altitudes of 30 and 70 kilometers, J.  
20 Geophys. Res., 78, 4451–4457, <https://doi.org/10.1029/jc078i021p04451>, 1973.

1 Flury, T., Hocke, K., Haefele, A., Kämpfer, N., and Lehmann, R.: Ozone depletion, water vapor increase, and  
2 PSC generation at midlatitudes by the 2008 major stratospheric warming, *J. Geophys. Res.*, 114,  
3 7903–14, <https://doi.org/10.1029/2009jd011940>, 2009.

4 Fritts, D. C. and Alexander, M. J.: Gravity wave dynamics and effects in the middle atmosphere, *Rev.*  
5 *Geophys.*, 41, 1003, <https://doi.org/10.1029/2001rg000106>, 2003.

6 Fusco, A. C. and Salby, M. L.: Interannual Variations of Total Ozone and Their Relationship to Variations of  
7 Planetary Wave Activity, *J. Climate*, 12, 1619–1629, <https://doi.org/10.1175/1520->  
8 0442(1999)012<1619:ivotoa>2.0.co;2, 1999.

9 García, O. E., Schneider, M., Redondas, A., González, Y., Hase, F., Blumenstock, T., and Sepúlveda, E.:  
0 Investigating the long-term evolution of subtropical ozone profiles applying ground-based FTIR  
1 spectrometry, *Atmos. Meas. Tech.*, 5, 2917–2931, <https://doi.org/10.5194/amt-5-2917-2012>, 2012.

2 Gaudel, A., Ancellet, G., and Godin-Beekmann, S.: Analysis of 20 Years of tropospheric ozone vertical  
3 profiles by lidar and ecc at observatoire de Haute Provence (OHP) at 44 N, 6.7 E, *Atmos. Environ.*,  
4 113, 78–89, <https://doi.org/10.1016/j.atmosenv.2015.04.028>, 2015.

5 Gelaro, R., McCarty, W., Suárez, M. J., Todling, R., Molod, A., Takacs, L., Randles, C. A., Darmenov, A.,  
6 Bosilovich, M. G., Reichle, R., Wargan, K., Coy, L., Cullather, R., Draper, C., Akella, S., Buchard,  
7 V., Conaty, A., Silva, A. M. da, Gu, W., Kim, G.-K., Koster, R., Lucchesi, R., Merkova, D., Nielsen,  
8 J. E., Partyka, G., Pawson, S., Putman, W., Rienecker, M., Schubert, S. D., Sienkiewicz, M., and  
9 Zhao, B.: The Modern-Era Retrospective Analysis for Research and Applications, Version 2  
10 (MERRA-2), *J. Climate*, 30, 5419–5454, <https://doi.org/10.1175/jcli-d-16-0758.1>, 2017.

11 Global Modeling and Assimilation Office (GMAO) , MERRA-2 inst3\_3d\_asm\_Nv: 3d,3-  
12 Hourly,Instantaneous,Model-Level,Assimilation,Assimilated Meteorological Fields V5.12.4,  
13 Greenbelt, MD, USA, Goddard Earth Sciences Data and Information Services Center (GES DISC),  
14 Accessed: [Nov 2021], 10.5067/WWQSQ8IVFW8, 2015a.

15 Global Modeling and Assimilation Office (GMAO), MERRA-2 inst3\_3d\_asm\_Np: 3d,3-  
16 Hourly,Instantaneous,Pressure-Level,Assimilation,Assimilated Meteorological Fields V5.12.4,  
17 Greenbelt, MD, USA, Goddard Earth Sciences Data and Information Services Center (GES DISC),  
18 Accessed: [Data Access Date], 10.5067/QBZ6MG944HW0, 2015b.

19 Goncharenko, L. and Zhang, S.-R.: Ionospheric signatures of sudden stratospheric warming: Ion temperature  
20 at middle latitude, *Geophys. Res. Lett.*, 35, L15804-4, <https://doi.org/10.1029/2008gl035684>, 2008.

21 Greening, K. and Hodgson, A.: Atmospheric analysis of the cold late February and early March 2018 over the

1 UK, Weather, 74, 79–85, <https://doi.org/10.1002/wea.3467>, 2019.

2 Haigh, J. D.: The role of stratospheric ozone in modulating the solar radiative forcing of climate, *Nature*, 370,  
3 544–546, <https://doi.org/10.1038/370544a0>, 1994.

4 Hitchcock, P. and Simpson, I. R.: The Downward Influence of Stratospheric Sudden Warmings\*, *J. Atmos.*  
5 *Sci.*, 71, 3856–3876, <https://doi.org/10.1175/jas-d-14-0012.1>, 2014.

6 Holton, J. R. and Lindzen, R. S.: An Updated Theory for the Quasi-Biennial Cycle of the Tropical Stratosphere,  
7 *J. Atmos. Sci.*, 29, 1076–1080, [https://doi.org/10.1175/1520-0469\(1972\)029<1076:autftq>2.0.co;2](https://doi.org/10.1175/1520-0469(1972)029<1076:autftq>2.0.co;2),  
8 1972.

9 Holton, J. R., Haynes, P. H., McIntyre, M. E., Douglass, A. R., Rood, R. B., and Pfister, L.: Stratosphere-  
0 troposphere exchange, *Rev. Geophys.*, 33, 403–439, <https://doi.org/10.1029/95rg02097>, 1995.

1 Houghton, J. T.: The stratosphere and mesosphere, *Q. J. R. Meteorol. Soc.*, 104, 1–29,  
2 <https://doi.org/doi.org/10.1002/qj.49710443902>, 1978.

3 Ineson, S., and A. A. Scaife.: The role of the stratosphere in the European climate response to El Niño, *Nature*  
4 *Geoscience*, 2, 32–36, doi:10.1038/ngeo381, 2008.

5 Jaeglé, L., Wood, R., & Wargan, K.: Multiyear composite view of ozone enhancements and stratosphere-to-  
6 troposphere transport in dry intrusions of northern hemisphere extratropical cyclones. *J. Geophys.*  
7 *Res.: Atmospheres*, 122. <https://doi.org/10.1002/2017JD027656>, 2017.

8 Johnson, B. J., Oltmans, S. J., Vömel, H., Smit, H. G. J., Deshler, T., and Kröger, C.: Electrochemical  
9 concentration cell (ECC) ozonesonde pump efficiency measurements and tests on the sensitivity to  
10 ozone of buffered and unbuffered ECC sensor cathode solutions, *J. Geophys. Res.*, 107, 7881,  
11 <https://doi.org/10.1029/2001jd000557>, 2002.

12 Karpechko, A. Y., Perlwitz, J., and Manzini, E.: A model study of tropospheric impacts of the Arctic ozone  
13 depletion 2011, *J. Geophys. Res.*, 119, 7999–8014, <https://doi.org/10.1002/2013jd021350>, 2014.

14 Karpechko, A. Y., Perez, A. C., Balmaseda, M., Tyrrell, N., and Vitart, F.: Predicting Sudden Stratospheric  
15 Warming 2018 and Its Climate Impacts With a Multimodel Ensemble, *Geophys. Res. Lett.*, 45, 2096–  
16 9, <https://doi.org/10.1029/2018gl081091>, 2018.

17 Kidston, J., Scaife, A. A., Hardiman, S. C., Mitchell, D. M., Butchart, N., Baldwin, M. P., and Gray, L. J.:  
18 Stratospheric influence on tropospheric jet streams, storm tracks and surface weather, *Nat. Geosci.*,  
19 8, 1–8, <https://doi.org/10.1038/ngeo2424>, 2015.

1 Knowland, K. E., Ott, L. E., Duncan, B. N., and Wargan, K.: Stratospheric Intrusion-Influenced Ozone Air  
2 Quality Exceedances Investigated in the NASA MERRA-2 Reanalysis, *Geophys. Res. Lett.*, 44,  
3 10,691-10,701, <https://doi.org/10.1002/2017gl074532>, 2017.

4 Komhyr, W. D.: Operations handbook-ozone measurements to 40-km altitude with Model 4A Electrochemical  
5 Concentration Cell (ECC) ozonesonaes (used with 1680-MHz radiosondes), 1986.

6 Korenkov, Y. N., Klimenko, V. V., Klimenko, M. V., Bessarab, F. S., Korenkova, N. A., Ratovsky, K. G.,  
7 Chernigovskaya, M. A., Shcherbakov, A. A., Sahai, Y., Fagundes, P. R., Jesus, R. de, Abreu, A. J.  
8 de, and Condor, P.: The global thermospheric and ionospheric response to the 2008 minor sudden  
9 stratospheric warming event, *J. Geophys. Res.*, 117, <https://doi.org/10.1029/2012ja018018>, 2012.

0 Lawrence, Z. D. and Manney, G. L.: Does the Arctic Stratospheric Polar Vortex Exhibit Signs of  
1 Preconditioning Prior to Sudden Stratospheric Warmings?, *J. Atmos. Sci.*, 77, 611–632,  
2 <https://doi.org/10.1175/jas-d-19-0168.1>, 2020.

3 Lee, S. H. and Butler, A. H.: The 2018–2019 Arctic stratospheric polar vortex, *Weather*, 294, 581–6,  
4 <https://doi.org/10.1002/wea.3643>, 2019.

5 Limpasuvan, V., Richter, J. H., Orsolini, Y. J., Stordal, F., and Kvissel, O.-K.: The roles of planetary and  
6 gravity waves during a major stratospheric sudden warming as characterized in WACCM, *J. Atmos.*  
7 *Sol.-Terr. Phys.*, 78–79, 84–98, <https://doi.org/10.1016/j.jastp.2011.03.004>, 2012.

8 Lindzen, R. S. and Holton, J. R.: A Theory of the Quasi-Biennial Oscillation, *J. Atmos. Sci.*, 25, 1095–1107,  
9 [https://doi.org/10.1175/1520-0469\(1968\)025<1095:atotqb>2.0.co;2](https://doi.org/10.1175/1520-0469(1968)025<1095:atotqb>2.0.co;2), 1968.

10 Logan, J. A.: Trends in the vertical distribution of ozone: An analysis of ozonesonde data, *J. Geophys. Res.*,  
11 99, 25, <https://doi.org/10.1029/94jd02333>, 1994.

12 Logan, J. A., Megretskaia, I. A., Miller, A. J., Tiao, G. C., Choi, D., Zhang, L., Stolarski, R. S., Labow, G. J.,  
13 Hollandsworth, S. M., Bodeker, G. E., Claude, H., Muer, D. de, Kerr, J. B., Tarasick, D. W., Oltmans,  
14 S. J., Johnson, B., Schmidlin, F., Staehelin, J., Viatte, P., and Uchino, O.: Trends in the vertical  
15 distribution of ozone: A comparison of two analyses of ozonesonde data, *J. Geophys. Res.*, 104, 26,  
16 <https://doi.org/10.1029/1999jd900300>, 1999.

17 Manney, G. L., Krüger, K., Pawson, S., Minschwaner, K., Schwartz, M. J., Daffer, W. H., Livesey, N. J.,  
18 Mlynczak, M. G., Remsberg, E. E., III, J. M. R., and Waters, J. W.: The evolution of the stratopause  
19 during the 2006 major warming: Satellite data and assimilated meteorological analyses, *J. Geophys.*  
20 *Res.*, 113, 1576–16, <https://doi.org/10.1029/2007jd009097>, 2008a.



- 1 Manney, G. L., Daffer, W. H., Strawbridge, K. B., Walker, K. A., Boone, C. D., Bernath, P. F., Kerzenmacher,  
2 T., Schwartz, M. J., Strong, K., Sica, R. J., Ger, K. K. Ü., Pumphrey, H. C., Lambert, A., Santee, M.  
3 L., Livesey, N. J., Remsberg, E. E., Mlynczak, M. G., and Russell, J. R. I.: The high Arctic in extreme  
4 winters: vortex, temperature, and MLS and ACE-FTS trace gas evolution, *Atmos. Chem. and Phys.*,  
5 8, 505–522, <https://doi.org/10.5194/acp-8-505-2008>, 2008b.
- 6 Manney, G. L., Schwartz, M. J., Krüger, K., Santee, M. L., Pawson, S., Lee, J. N., Daffer, W. H., Fuller, R.  
7 A., and Livesey, N. J.: Aura Microwave Limb Sounder observations of dynamics and transport during  
8 the record-breaking 2009 Arctic stratospheric major warming, *Geophys. Res. Lett.*, 36, 581–5,  
9 <https://doi.org/10.1029/2009gl038586>, 2009a.
- 0 Manney, G. L., Harwood, R. S., MacKenzie, I. A., Minschwaner, K., Allen, D. R., Santee, M. L., Walker, K.  
1 A., Hegglin, M. I., Lambert, A., Pumphrey, H. C., Bernath, P. F., Boone, C. D., Schwartz, M. J.,  
2 Livesey, N. J., Daffer, W. H., and Fuller, R. A.: Satellite observations and modeling of transport in  
3 the upper troposphere through the lower mesosphere during the 2006 major stratospheric sudden  
4 warming, *Atmos. Chem. and Phys.*, 9, 4775–4795, <https://doi.org/10.5194/acp-9-4775-2009>, 2009b.
- 5 Manney, G. L., Lawrence, Z. D., Santee, M. L., Livesey, N. J., Lambert, A., and Pitts, M. C.: Polar processing  
6 in a split vortex: Arctic ozone loss in early winter 2012/2013, *Atmos. Chem. and Phys.*, 15, 5381–  
7 5403, <https://doi.org/10.5194/acp-15-5381-2015>, 2015.
- 8 Marsh, D. R., Mills, M. J., Kinnison, D. E., Lamarque, J.-F., Calvo, N., and Polvani, L. M.: Climate Change  
9 from 1850 to 2005 Simulated in CESM1(WACCM), *J. Climate*, 26, 7372–7391,  
10 <https://doi.org/10.1175/jcli-d-12-00558.1>, 2013.
- 11 Martineau, P., Wright, J. S., Zhu, N., and Fujiwara, M.: Zonal-mean data set of global atmospheric reanalyses  
12 on pressure levels, 10, 1925–1941, <https://doi.org/10.5194/essd-10-1925-2018>, 2018.
- 13 Martius, O., Polvani, L. M., and Davies, H. C.: Blocking precursors to stratospheric sudden warming events,  
14 *Geophys. Res. Lett.*, 36, 581–5, <https://doi.org/10.1029/2009gl038776>, 2009.
- 15 Matsuno, T.: A dynamical model of the stratospheric sudden warming, *J. Atmos. Sci.*, 28, 1479–1494,  
16 [https://doi.org/https://doi.org/10.1175/1520-0469\(1971\)028<1479:ADMOTS>2.0.CO;2](https://doi.org/https://doi.org/10.1175/1520-0469(1971)028<1479:ADMOTS>2.0.CO;2), 1971.
- 17 McDonald, M. K., Turnbull, D. N., and Donovan, D. P.: Steller Brewer, ozonesonde, and DIAL measurements  
18 of Arctic O<sub>3</sub> column over Eureka, N.W.T. during 1996 winter/spring, *Geophys. Res. Lett.*, 26, 2383–  
19 2386, <https://doi.org/10.1029/1999gl900506>, 1999.
- 20 Molod, A., Takacs, L., Suarez, M., and Bacmeister, J.: Development of the GEOS-5 atmospheric general  
21 circulation model: evolution from MERRA to MERRA2, *Geosci. Model Dev.*, 8, 1339–1356,

1 <https://doi.org/10.5194/gmd-8-1339-2015>, 2015.

2 Nakamura, N.: Two-Dimensional Mixing, Edge Formation, and Permeability Diagnosed in an Area  
3 Coordinate., J. Atmos. Sci., 53, 1524–1537,  
4 [https://doi.org/10.1175/15200469\(1996\)053<1524:tdmefa>2.0.co;2](https://doi.org/10.1175/15200469(1996)053<1524:tdmefa>2.0.co;2), 1996.

5 Nowack, P. J., Abraham, N. L., Maycock, A. C., Braesicke, P., Gregory, J. M., Joshi, M. M., Osprey, A., and  
6 Pyle, J. A.: A large ozone-circulation feedback and its implications for global warming assessments,  
7 Nat. Clim. Chang., 5, 41–45, <https://doi.org/10.1038/nclimate2451>, 2015.

8 Palmeiro, F. M., Barriopedro, D., García-Herrera, R., and Calvo, N.: Comparing Sudden Stratospheric  
9 Warming Definitions in Reanalysis Data\*, J. Climate, 28, 6823–6840, [https://doi.org/10.1175/jcli-d-](https://doi.org/10.1175/jcli-d-15-0004.1)  
0 [15-0004.1](https://doi.org/10.1175/jcli-d-15-0004.1), 2015.

1 Polvani, L. M. and Waugh, D. W.: Upward Wave Activity Flux as a Precursor to Extreme Stratospheric Events  
2 and Subsequent Anomalous Surface Weather Regimes., J. Climate, 17, 3548–3554,  
3 [https://doi.org/10.1175/1520-0442\(2004\)017<3548:uwafaa>2.0.co;2](https://doi.org/10.1175/1520-0442(2004)017<3548:uwafaa>2.0.co;2), 2004.

4 Ramaswamy, V., Schwarzkopf, M. D., and Randel, W. J.: Fingerprint of ozone depletion in the spatial and  
5 temporal pattern of recent lower-stratospheric cooling, Nature, 382, 616–618,  
6 <https://doi.org/10.1038/382616a0>, 1996.

7 Randel, W. J.: Global variations of zonal mean ozone during stratospheric warming events, J. Atmos. Sci., 50,  
8 3308–3321, 1993.

9 Randel, W. J., Wu, F., and Stolarski, R.: Changes in Column Ozone Correlated with the Stratospheric EP Flux,  
10 J. Meteorol. Soc. Jpn. Ser. II, 80, 849–862, <https://doi.org/10.2151/jmsj.80.849>, 2002.

11 Rao, J., Ren, R., Chen, H., Yu, Y., and Zhou, Y.: The Stratospheric Sudden Warming Event in February 2018  
12 and its Prediction by a Climate System Model, J. Geophys. Res., 123, 34–44,  
13 <https://doi.org/10.1029/2018jd028908>, 2018.

14 Rao, J., Garfinkel, C. I., Chen, H., and White, I. P.: The 2019 New Year Stratospheric Sudden Warming and  
15 Its Real-Time Predictions in Multiple S2S Models, J. Geophys. Res., 124, 11155–11174,  
16 <https://doi.org/10.1029/2019jd030826>, 2019.

17 Rao, T. N.: Climatology of UTLS ozone and the ratio of ozone and potential vorticity over northern Europe,  
18 J. Geophys. Res., 108, 3451–10, <https://doi.org/10.1029/2003jd003860>, 2003.

19 Rao, T. N., Arvelius, J., Kirkwood, S., and Gathen, P. von der: Climatology of ozone in the troposphere and

1 lower stratosphere over the European Arctic, *Adv. Space Res.*, 34, 754–758,  
2 <https://doi.org/10.1016/j.asr.2003.05.055>, 2004.

3 Rienecker, M. M., Suárez, M. J., Gelaro, R., Todling, R., Bacmeister, J., Liu, E., Bosilovich, M. G., Schubert,  
4 S. D., Takacs, L., Kim, G.-K., Bloom, S., Chen, J., Collins, D., Conaty, A., Silva, A. da, Gu, W.,  
5 Joiner, J., Koster, R. D., Lucchesi, R., Molod, A., Owens, T., Pawson, S., Pegion, P., Redder, C. R.,  
6 Reichle, R., Robertson, F. R., Ruddick, A. G., Sienkiewicz, M., and Woollen, J.: MERRA: NASA's  
7 Modern-Era Retrospective Analysis for Research and Applications, *J. Climate*, 24, 3624–3648,  
8 <https://doi.org/10.1175/jcli-d-11-00015.1>, 2011.

9 Rodgers, C. D.: *Inverse Methods for Atmospheric Sounding - Theory and Practice*, Series on Atmospheric  
0 Oceanic and Planetary Physics, <https://doi.org/10.1142/9789812813718>, 2000.

1 Rodgers, C. D. and Connor, B. J.: Intercomparison of remote sounding instruments, *J. Geophys. Res.*, 108,  
2 n/a-n/a, <https://doi.org/10.1029/2002jd002299>, 2003.

3 Romanowsky, E., Handorf, D., Jaiser, R., Wohltmann, I., Dorn, W., Ukita, J., Cohen, J., Dethloff,  
4 K., and Rex, M.: The role of stratospheric ozone for Arctic-midlatitude linkages, *Scientific Reports*,  
5 9, 1–7, <https://doi.org/10.1038/s41598-019-43823-1>, 2019.

6 Rothman, L. S., Gordon, I. E., Barbe, A., Benner, D. C., Bernath, P. F., Birk, M., Boudon, V., Brown, L. R.,  
7 Campargue, A., Champion, J. P., Chance, K., Coudert, L. H., Dana, V., Devi, V. M., Fally, S., Flaud,  
8 J. M., Gamache, R. R., Goldman, A., Jacquemart, D., Kleiner, I., Lacome, N., Lafferty, W. J., Mandin,  
9 J. Y., Massie, S. T., Mikhailenko, S. N., Miller, C. E., Moazzen-Ahmadi, N., Naumenko, O. V.,  
10 Nikitin, A. V., Orphal, J., Perevalov, V. I., Perrin, A., Predoi-Cross, A., Rinsland, C. P., Rotger, M.,  
11 Šimečková, M., Smith, M. A. H., Sung, K., Tashkun, S. A., Tennyson, J., Toth, R. A., Vandaele, A.  
12 C., and Auwera, J. V.: The HITRAN 2008 molecular spectroscopic database, *J. Quant. Spectrosc.*  
13 *and Radiat. Transf.*, 110, 533–572, <https://doi.org/10.1016/j.jqsrt.2009.02.013>, 2009.

14 Scheiben, D., Straub, C., Hocke, K., Forkman, P., and Kämpfer, N.: Observations of middle atmospheric  
15 H<sub>2</sub>O and O<sub>3</sub> during the 2010 major sudden stratospheric warming by a network of microwave  
16 radiometers, *Atmospheric Chemistry and Physics*, 12, 7753–7765, [https://doi.org/10.5194/acp-12-](https://doi.org/10.5194/acp-12-7753-2012)  
17 [7753-2012](https://doi.org/10.5194/acp-12-7753-2012), 2012.

18 Scherhag, R.: Die explosionsartigen Stratosphärenwärmungen des Spätwinters, *Ber. Det. Wetterdienstes*,  
19 38, 51–63, 1952.

20 Schoeberl, M. R.: Stratospheric Warmings: Observations and Theory, 16, 521,  
21 <https://doi.org/10.1029/rg016i004p00521>, 1978.

1 Schranz, F., Hagen, J., Stober, G., Hocke, K., Murk, A., and Kämpfer, N.: Small-scale variability of  
2 stratospheric ozone during the sudden stratospheric warming 2018/2019 observed at Ny-Ålesund,  
3 Svalbard, *Atmospheric Chemistry and Physics*, 20, 10791–10806, [https://doi.org/10.5194/acp-20-](https://doi.org/10.5194/acp-20-10791-2020)  
4 10791-2020, 2020.

5 Scott, R. K. and Polvani, L. M.: Stratospheric control of upward wave flux near the tropopause, *Geophys.*  
6 *Res. Lett.*, 31, 581–4, <https://doi.org/10.1029/2003gl017965>, 2004.

7 Shangguan, M., Wang, W., and Jin, S.: Variability of temperature and ozone in the upper troposphere and  
8 lower stratosphere from multi-satellite observations and reanalysis data, *Atmos. Chem. Phys.*, 19,  
9 6659–6679, <https://doi.org/10.5194/acp-19-6659-2019>, 2019.

0 Siskind, D. E., Eckermann, S. D., Coy, L., McCormack, J. P., and Randall, C. E.: On recent interannual  
1 variability of the Arctic winter mesosphere: Implications for tracer descent, *Geophys. Res. Lett.*, 34,  
2 498–5, <https://doi.org/10.1029/2007gl029293>, 2007.

3 Smit, H. G. J., Straeter, W., Johnson, B. J., Oltmans, S. J., Davies, J., Tarasick, D. W., Hoegger, B., Stubi,  
4 R., Schmidlin, F. J., Northam, T., Thompson, A. M., Witte, J. C., Boyd, I., and Posny, F.:  
5 Assessment of the performance of ECC-ozonesondes under quasi-flight conditions in the  
6 environmental simulation chamber: Insights from the Juelich Ozone Sonde Intercomparison  
7 Experiment (JOSIE), *J. Geophys. Res.*, 112, 563–18, <https://doi.org/10.1029/2006jd007308>, 2007.

8 Smith, K. L. and Polvani, L. M.: The surface impacts of Arctic stratospheric ozone anomalies, *Environ. Res.*  
9 *Lett.*, 9, 074015–9, <https://doi.org/10.1088/1748-9326/9/7/074015>, 2014.

10 Sterling, C. W., Johnson, B. J., Oltmans, S. J., Smit, H. G. J., Jordan, A. F., Cullis, P. D., Hall, E. G.,  
11 Thompson, A. M., and Witte, J. C.: Homogenizing and Estimating the Uncertainty in NOAA’s Long  
12 Term Vertical Ozone Profile Records Measured with the Electrochemical Concentration Cell  
13 Ozonesonde, *Atmos. Meas. Tech. Discuss.*, 1–39, <https://doi.org/10.5194/amt-2017-397>, 2017.

14 Stolarski, R. S.: History of the Study of Atmospheric Ozone, *Ozone Science Engineering*, 23, 421–428,  
15 <https://doi.org/http://doi.org/10.1080/01919510108962025>, 2001.

16 Strahan, S.E., A.R. Douglass, and S.D. Steenrod, Chemical and dynamical impacts of stratospheric sudden  
17 warmings on Arctic ozone variability, *J. Geophys. Res. Atmos.*, 121, 11,836–11,851,  
18 doi:10.1002/2016JD025128, 2016.

19 Tao, M., Konopka, P., Ploeger, F., Groß, J. U., Müller, R., Volk, C. M., Walker, K. A., and Riese, M.: Impact  
20 of the 2009 major sudden stratospheric warming on the composition of the stratosphere, *Atmospheric*  
21 *Chemistry and Physics*, 15, 8695–8715, <https://doi.org/10.5194/acp-15-8695-2015>, 2015.

- 1 Tarasick, D. W. and Bottenheim, J. W.: Surface ozone depletion episodes in the Arctic and Antarctic from  
2 historical ozonesonde records, *Atmos Chem Phys*, 2, 197–205, [https://doi.org/10.5194/acp-2-197-](https://doi.org/10.5194/acp-2-197-2002)  
3 2002, 2002.
- 4 Tarasick, D. W., Davies, J., Smit, H. G. J., and Oltmans, S. J.: A re-evaluated Canadian ozonesonde record:  
5 measurements of the vertical distribution of ozone over Canada from 1966 to 2013, *Atmos. Meas.*  
6 *Tech.*, 9, 195–214, <https://doi.org/10.5194/amt-9-195-2016>, 2016.
- 7 Tegtmeier, S., M. Rex, I. Wohltmann, and K. Krüger, Relative importance of dynamical and chemical  
8 contributions to Arctic wintertime ozone, *Geophys. Res. Lett.*, 35, L17801,  
9 [doi:10.1029/2008GL034250](https://doi.org/10.1029/2008GL034250), 2008.
- 0 Thurairajah, B., Collins, R. L., Harvey, V. L., Lieberman, R. S., Gerding, M., Mizutani, K., and Livingston, J.  
1 M.: Gravity wave activity in the Arctic stratosphere and mesosphere during the 2007–2008 and 2008–  
2 2009 stratospheric sudden warming events, *J. Geophys. Res.*, 115, S637-17,  
3 <https://doi.org/10.1029/2010jd014125>, 2010.
- 4 Tiao, G. C., Reinsel, G. C., Pedrick, J. H., Allenby, G. M., Mateer, C. L., Miller, A. J., and DeLuisi, J. J.: A  
5 statistical trend analysis of ozonesonde data, *J. Geophys. Res.*, 91, 13121–13136,  
6 <https://doi.org/10.1029/jd091id12p13121>, 1986.
- 7 Tripathi, O. P., Baldwin, M., Perez, A. C., Charron, M., Eckermann, S. D., Gerber, E., Harrison, R. G., Jackson,  
8 D. R., Kim, B.-M., Kuroda, Y., Lang, A., Mahmood, S., Mizuta, R., Roff, G., Sigmond, M., and Son,  
9 S.-W.: The predictability of the extratropical stratosphere on monthly time-scales and its impact on  
10 the skill of tropospheric forecasts, *Q. J. R. Meteorol. Soc.*, 141, 987–1003,  
11 <https://doi.org/10.1002/qj.2432>, 2015.
- 12 Vigouroux, C., Mazière, M. D., Demoulin, P., Servais, C., Hase, F., Blumenstock, T., Kramer, I., Schneider,  
13 M., Mellqvist, J., Strandberg, A., Velazco, V., Notholt, J., Sussmann, R., Stremme, W., Rockmann,  
14 A., Gardiner, T., Coleman, M., and Woods, P.: Evaluation of tropospheric and stratospheric ozone  
15 trends over Western Europe from ground-based FTIR network observations, *Atmos. Chem. Phys.*, 8,  
16 6865–6886, <https://doi.org/10.5194/acp-8-6865-2008>, 2008.
- 17 Vigouroux, C., Blumenstock, T., Coffey, M., Errera, Q., García, O., Jones, N. B., Hannigan, J. W., Hase, F.,  
18 Liley, B., Mahieu, E., Mellqvist, J., Notholt, J., Palm, M., Persson, G., Schneider, M., Servais, C.,  
19 Smale, D., Thölix, L., and Mazière, M. D.: Trends of ozone total columns and vertical distribution  
20 from FTIR observations at eight NDACC stations around the globe, *Atmos. Chem. Phys.*, 15, 2915–  
21 2933, <https://doi.org/10.5194/acp-15-2915-2015>, 2015.
- 22 Wallace, J. M.: General circulation of the tropical lower stratosphere, *Rev. Geophys.*, 11, 191–222,



1  
2  
3  
4

**Table I.** Site locations for NDACC FTIRs and ozonesondes. Uncertainties of FTIRs at three sites with ozonesondes are given by averaged subtraction and standard deviation of ozonesondes from the retrieved ozone from FTIR, as uncertainty of partial column ozone (PCO) in both ground to 30km and 10 to 30 km.

station	Longitude	Latitude	Solar FTIR Time period	Ozonesonde Availability period	% PCO uncertainties (Ground -30 km)	% PCO Uncertainties (10 km -30km)
Eureka	274	80	2006-now	1992-now	7% +/- 7%	1% +/- 7%
Ny-Ålesund	12	79	1995-now	1992-now	2% +/- 4%	7% +/- 8%
Thule	291	77	1999-now	1991-2016 (sparse)	3% +/- 6%	3% +/- 6%
Summit Station	39	72	-	2005-2017	-	-
Harestua	11	60	2009-now	-	-	-
Kiruna	20	68	1997-now	-	-	-

5

**Table II.** SSWs dates, duration, magnitude, and the duration of polar vortex from 2004 to 2020. The number of easterly days at 10 hPa over 60 N is shown as the duration SSW. The magnitude of SSWs is defined by the minimum zonal-mean zonal wind at 10hPa over 60 N during each SSW. The total number of easterly days associated with the event is not necessarily consecutive. The duration of polar vortex recovery is defined as the number of days that the zonal averaged EPV takes to reach the climatological zonal EPV.

SSWs date	Number of easterly days at 10 hPa over 60 N	Minimum zonal-mean zonal wind at 10hPa over 60°N (m/s)	Vortex recovery (days)
21 Jan 2006	26	-26	36
22 Feb 2008	16	-15	35
24 Jan 2009	30	-29	45
6 Jan 2013	22	-13	45
12 Feb 2018	19	-24	45
2 Jan 2019	19	-10	30



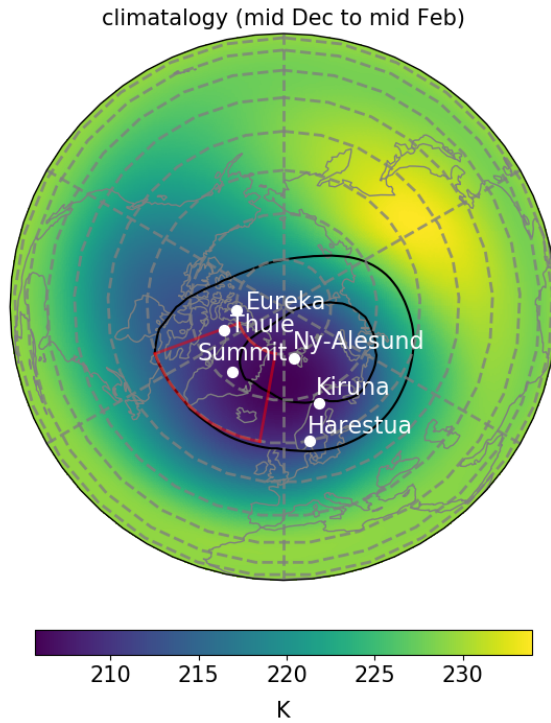


**Figure 1.** The climatology of temperature at 10 hPa and potential vorticity (PV) at the potential temperature of 850 K during wintertime (DJF) over the northern hemisphere. The climatology is based on non-SSW years from 2004 to 2019. The map coloring shows the average winter temperature. The black contour lines are 600 and 800 PV units ( $10^{-6} \text{ K m}^2 \text{ Kg}^{-1} \text{ s}^{-1}$ ). The locations of the observational sites are shown as white dots. Greenland sector is shown by the red polygon.

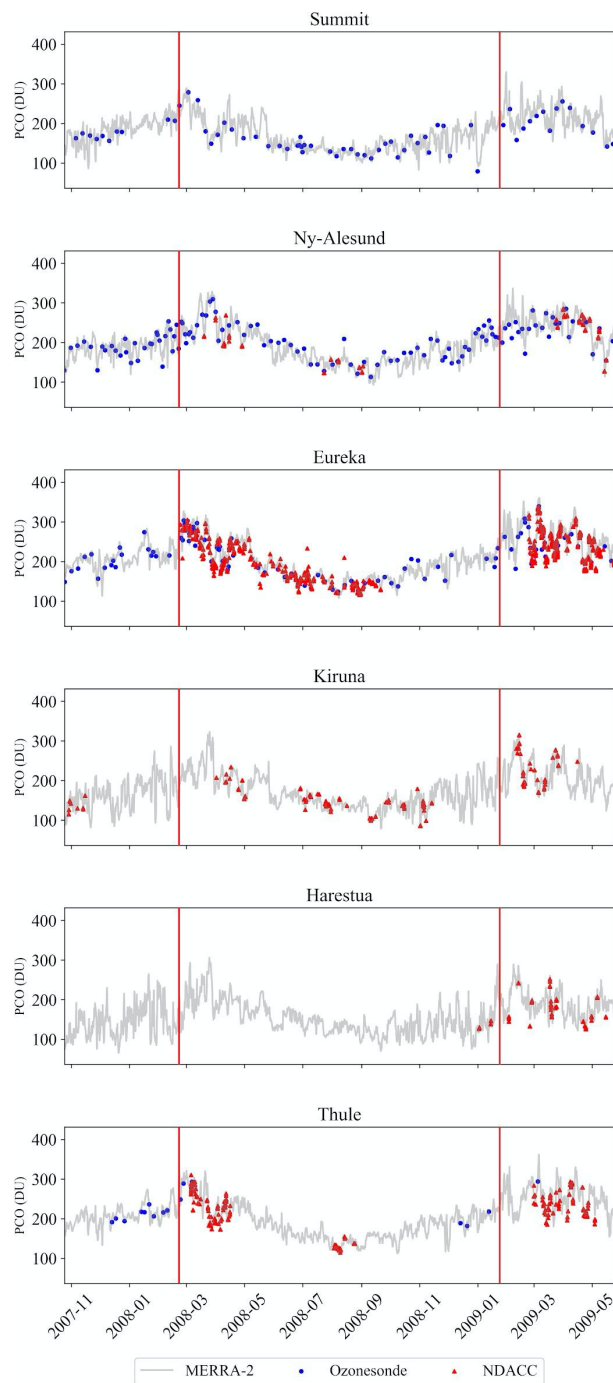


**Figure 2.** Time series of 3 hourly partial column ozone (PCO) of ground to 20 km derived from MERRA-2, solar FTIR, and ozonesondes at the study sites from winter 2007 to spring 2009. MERRA-2 is shown as the gray line. NDACC FTIR data and ozonesondes are shown as red triangles and blue circles,

respectively. The vertical red lines highlight the dates of the 2008 and 2009 SSWs.

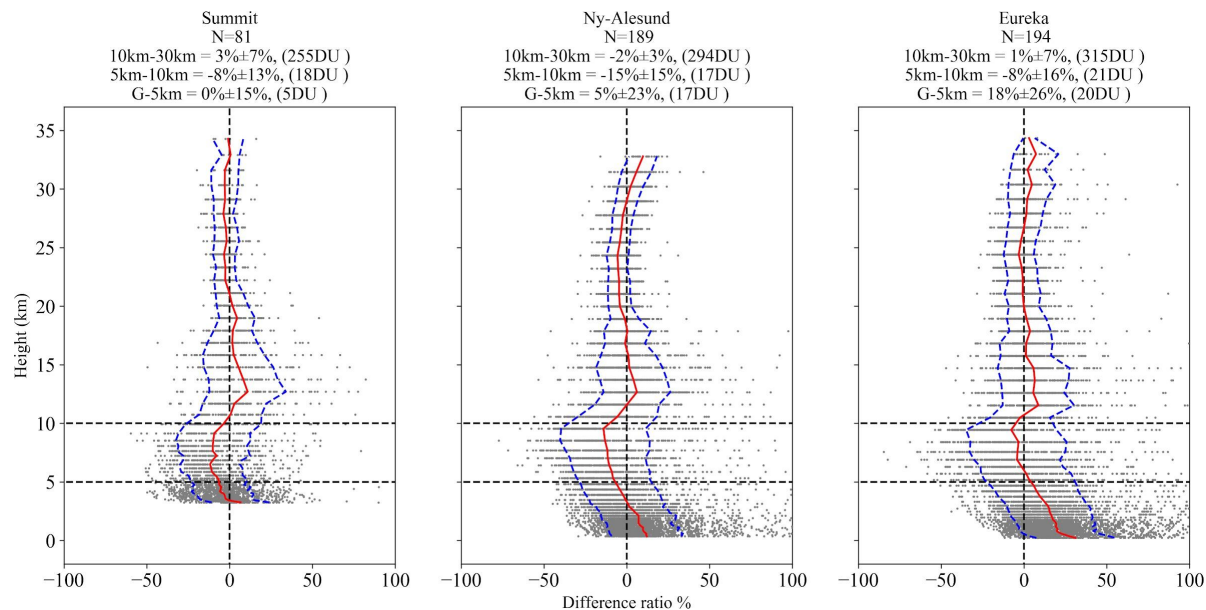


**Figure 3.** Relative differences of ozonesonde and MERRA-2 at each layer at three sites from 1 Dec to 1 May for six year of SSWs. The relative difference is the subtraction of ozonesonde from MERRA-2 ozone dataset divided by ozonesonde for each layer. The normalized mean bias is shown as the red line. The standard deviation of the relative differences from the normalized mean biases are shown with the blue lines. The number of coincident ozonesonde and MERRA-2 comparisons between 1st Dec and 1st May for the six years of SSWs (N) is shown under each site name. The mean and standard deviation of PCO relative differences for 3 layers: 10km-30km, 5km-10km, Ground-5km are summarized for each site. The average PCO value for each layer is shown in parentheses.

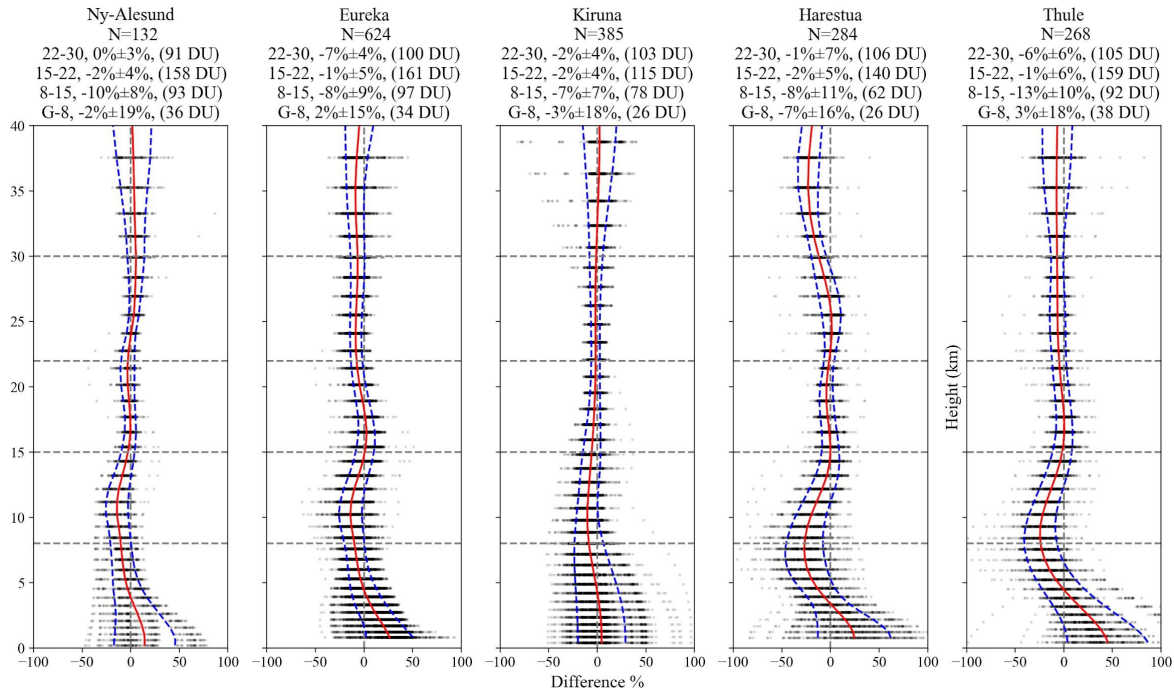


**Figure 4.** Same as Figure 3 but for relative differences of FTIR retrieved ozone from MERRA-2. Statistical summaries of the MERRA-2 and NDACC comparisons in four layers of ground to 8 km, 8km-15km, 15km -22km, and 22km- 30km for each station are shown on top of each plot.

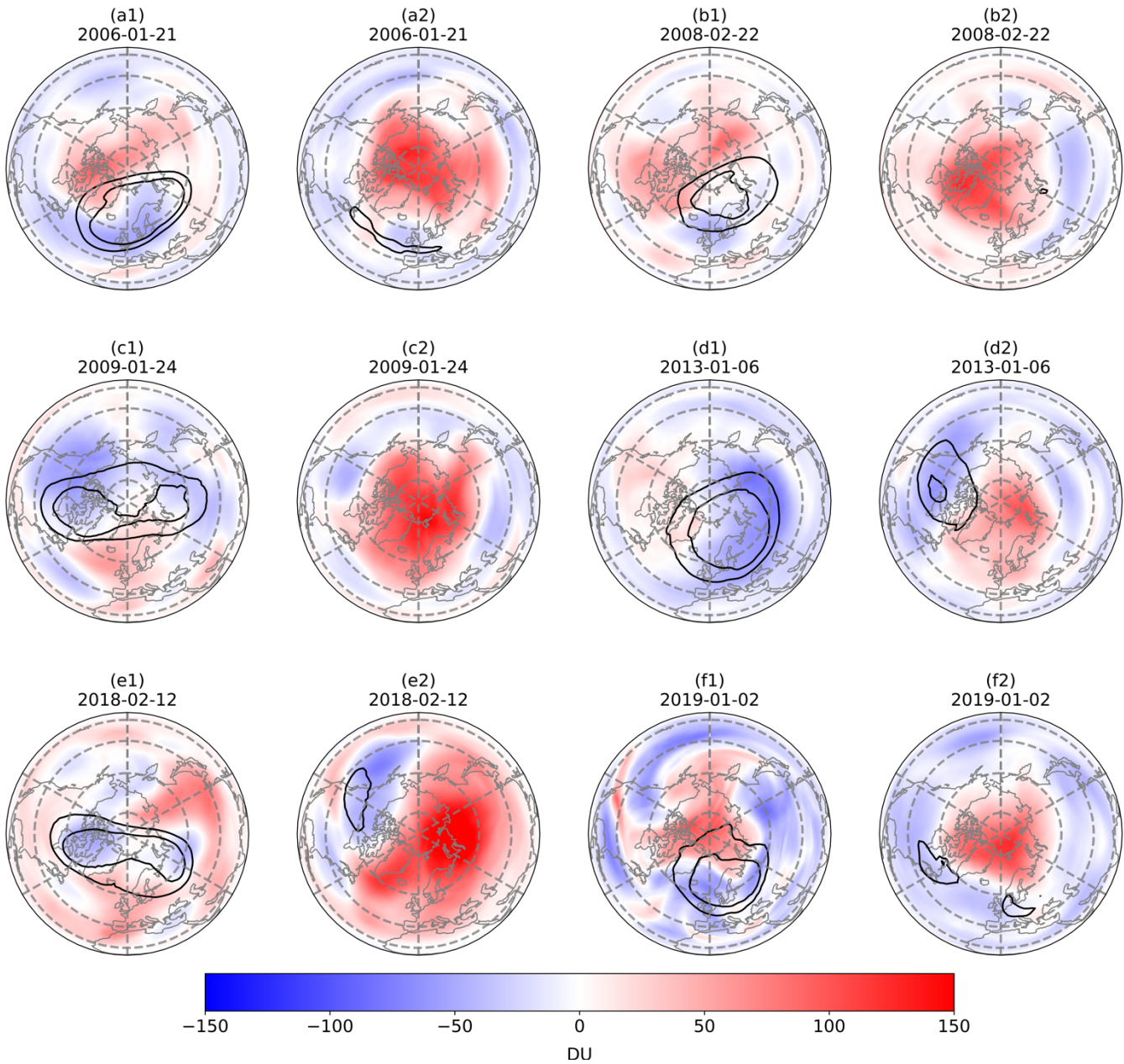


**Figure 5.** The anomaly TCO average over 15 days prior (alphabet1, first and third columns) and 15 days after each SSW (alphabet2, second and fourth columns) compared to climatology on non-SSW years. PEV at the potential temperature of 850k is averaged for the same period similar to TCO.

Contour lines show the EPV map at 600 and 800  $10^{-6} \text{ K m}^2 \text{ Kg}^{-1} \text{ s}^{-1}$ .

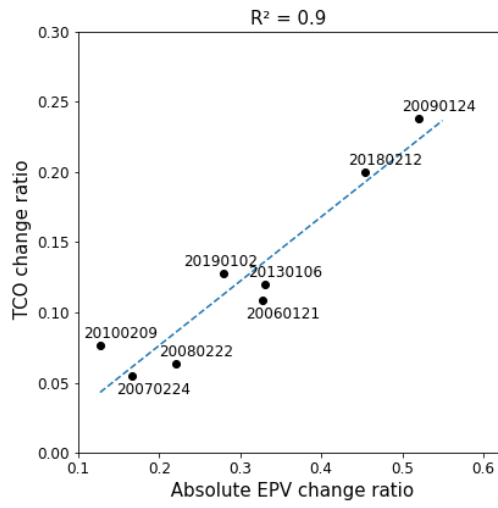


**Figure 6.** The zonally averaged EPV change ratio at the potential temperature of 850 K against the corresponding change in TCO for six studied SSW as well as less persistent major SSWs in 2007 and 2010. The ratio of change for each variable is estimated as the average of 15 days after SSWs subtracted by the average of 15 days before the SSWs and divided by the average of 15 days before.



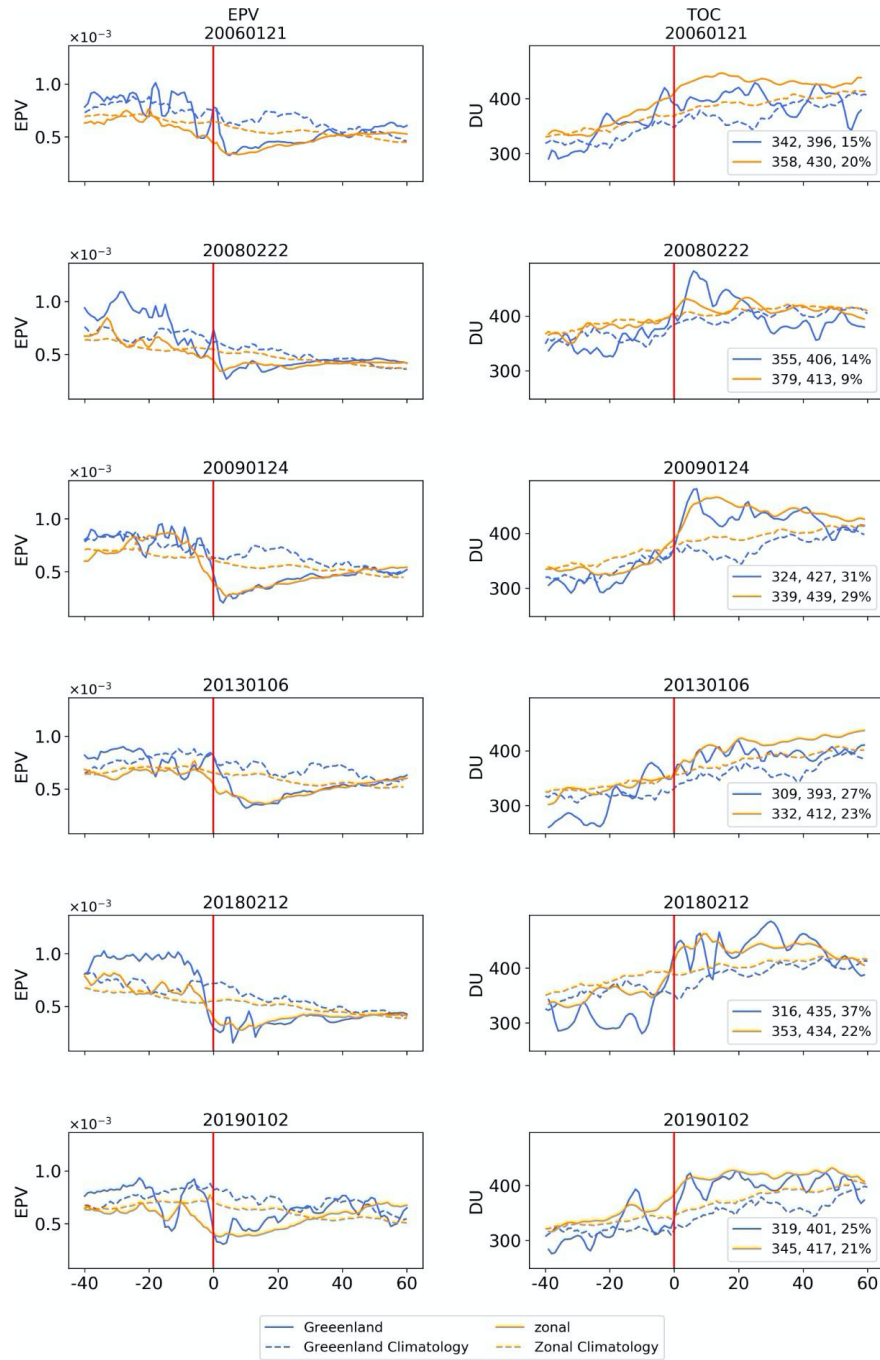


**Figure 7.** EPV at the potential temperature of 850k (first column) and TCO (second column) over the Arctic zonal mean 60-80N (orange line) and Greenland sector (blue line) during 40 days before and 60 days after each SSWs (each row). Climatology of EPV and TCO for the zonal and Greenland sector are shown in orange and blue dashed lines, respectively. The average Total Column ozone (TCO) during 40

days before and 60 days after, and the percentage of change for each SSWs are shown in the bottom corner of the second column.

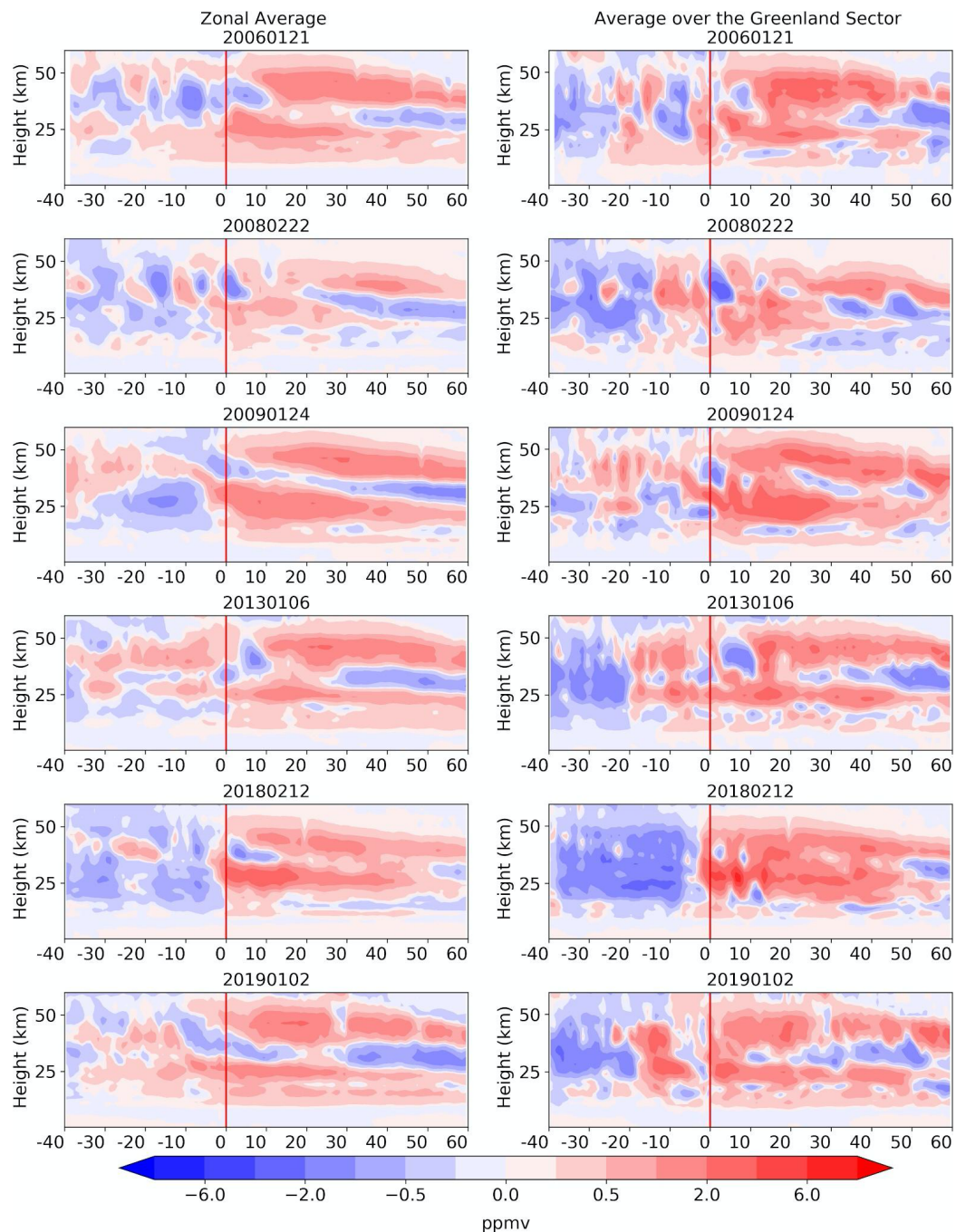


**Figure 8.** The cross section of ozone anomaly during 40 days before to 60 day of each SSWs averaged over the latitude band 60°N-80°N and Greenland sector (60°N-80°N, 10°W-70°W). The vertical red line shows the SSWs incident date. Climatology was created using non-SSWs years since 2004. The vertical coordinate is the log-pressure height.

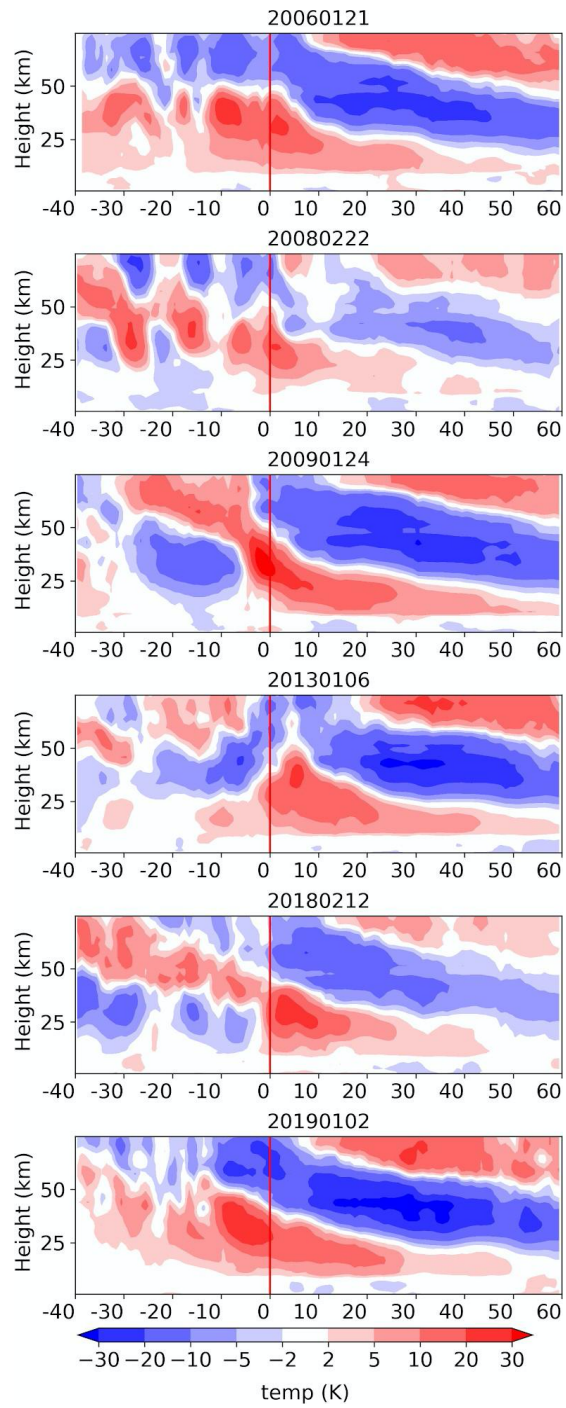


**Figure 9.** Similar to figure 8 but for the temperature anomaly for zonal average.

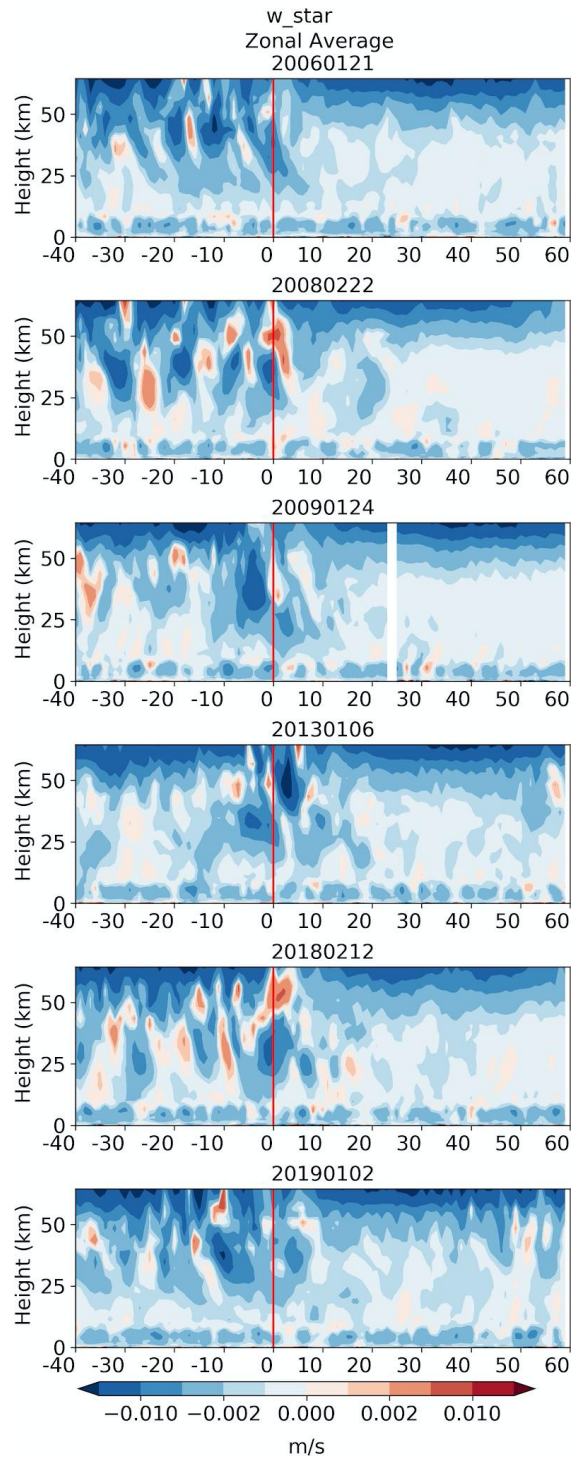


**Figure 10.** Similar to figure 8 but for the of the vertical component of the residual circulation,  $\underline{w}^*$ , for zonal average.

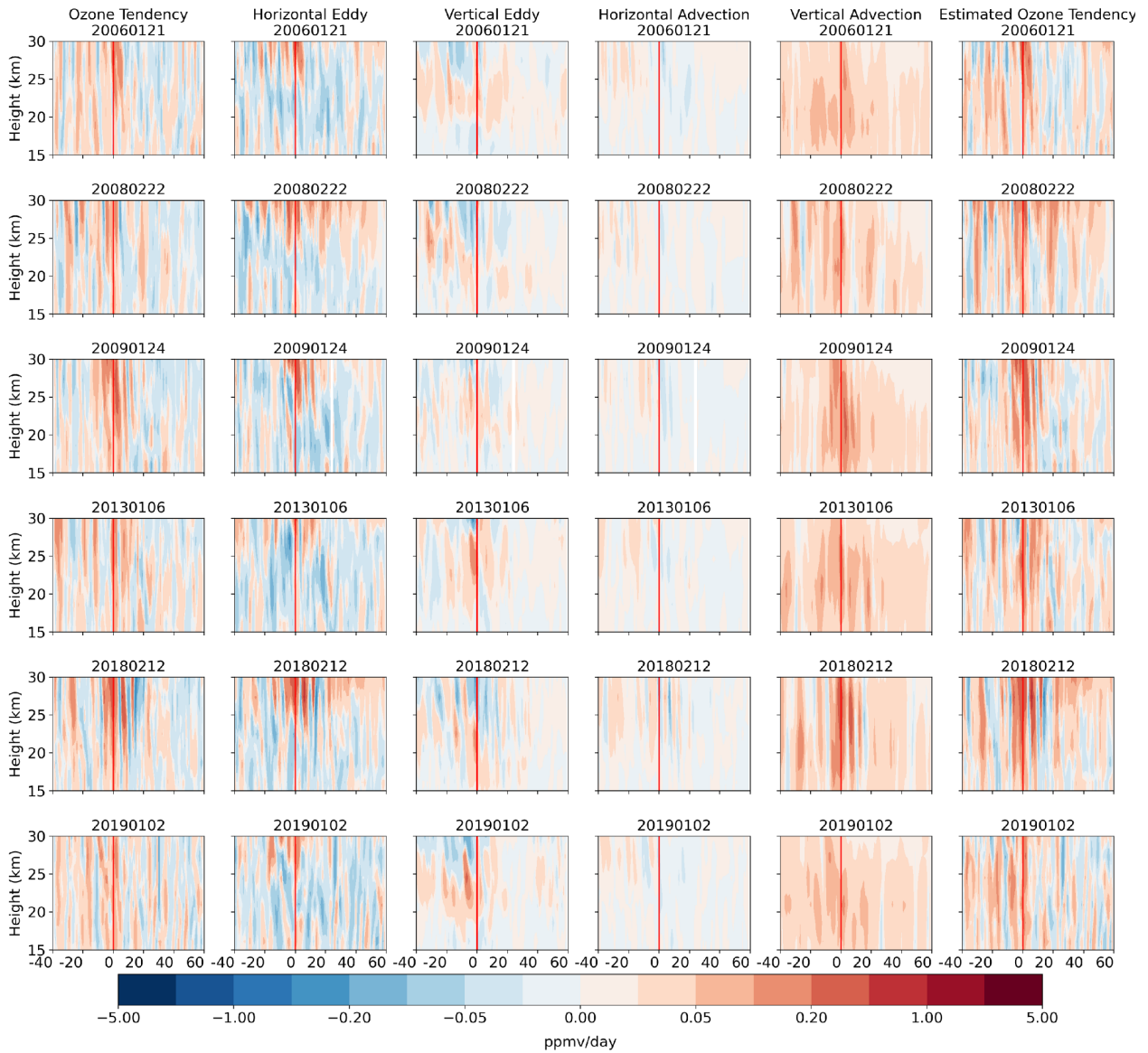


**Figure 11.** Same as Figure 8 for ozone tendency, horizontal and vertical component of eddy mixing, and horizontal ( $-\bar{v}^* \bar{x}_y$ ) and vertical ( $-\bar{w}^* \bar{x}_z$ ) component of mean advection, and the indirect ozone tendency using the right-hand side of equation (2). Summing four middle columns leads to the estimated ozone tendency on the sixth column. The vertical axis is the log-pressure height.

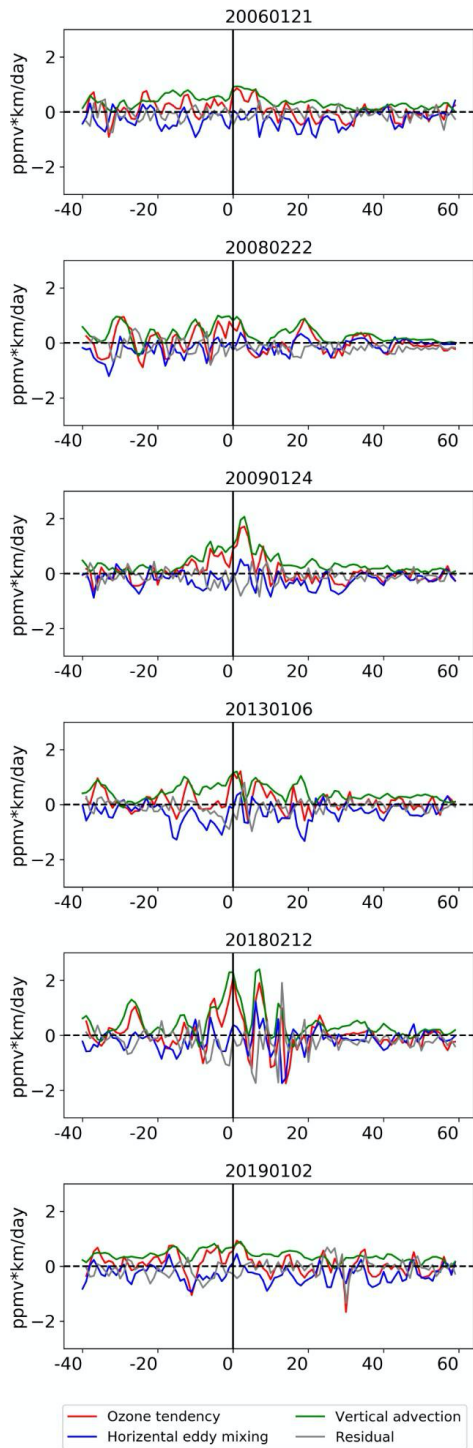


**Figure 12.** Time series of vertically integrated major elements of tracer continuity equation 2 from 15km to 30 km (Andrews et al, 1987). Ozone tendency is shown as the red line. The horizontal component of eddy mixing is shown in blue line, the vertical component of vertical advection, is shown in the green line. The residual of all elements of tracer continuity is shown in the gray line.